Bruno Gonçalo Guerreiro da Silva

HYDRODINAMICS DRIVEN DESIGN OF COASTAL ARTIFICAL REEFS

UNIVERSITY OF ALGARVE

Faculty of Sciences and Technology

2022

Bruno Gonçalo Guerreiro da Silva

HYDRODINAMICS DRIVEN DESIGN OF COASTAL ARTIFICAL REEFS

Master's in marine and coastal systems

This master thesis was realized

under the supervision of:

Professor. Dr. Duarte Nuno Ramos Duarte

Professor. Dr. Eduardo Nuno Borges Pereira

UNIVERSITY OF ALGARVE

Faculty of Sciences and Technology

2022

HYDRODINAMICS DRIVEN DESIGN OF COASTAL ARTIFICAL REEFS

Declaração de autoria de trabalho, declaro ser o autor desta tese de mestrado, que é original e inédito. Autores e trabalhos consultados estão devidamente citados no texto e constam da listagem de referências incluída.

I hereby declare to be the author of this master thesis, which is original and unpublished. Authors and works consulted are properly cited in the text and included in the reference list.

(Bruno Gonçalo Guerreiro da Silva)

HYDRODINAMICS DRIVEN DESIGN OF COASTAL ARTIFICAL REEFS

(Bruno Gonçalo Guerreiro da Silva)

Acknowledgements

I want to thank Professors Duarte Duarte and Eduardo Pereira for their support and guidance during this assignment.

I also want to thank my parents and brothers, Cristiano Silva and Sandra Silva, Lourenço Silva, and Salvador Silva for all the support and advice.

I also want to show my deepest thanks to my girlfriend Melanie Silva Silva for being there every single moment for me.

I also would like to thank to Dmytro Maslov for all the good advice, help and for being a good friend.

I would also like to thank Dr. Weizhi Wang, Dr. Ronja and all the REEF3D® team from the Marine Civil Engineering Civil and Environmental Engineering Dep. NTNU, Trondheim, Norway, for helping in the development of my project.

At least but not less important I want to thank to Professor Doctor Oscar Ferreira and Doctor Juan Luis Garzon Hervas for provide data that were essential for the completion of this master's thesis.

Resumo

Os sistemas marinhos e costeiros encontram-se sujeitos a uma enorme pressão humana, incluindo poluição, pesca excessiva, o efeito de espécies invasoras entre outros. Estes tipos de pressões resultam do facto de uma grande parte da população mundial viver perto da costa, e da grande profusão de atividades humanas que hoje se desenvolvem no mar. Quando os sistemas marinhos e costeiros entram em conflito com o desenvolvimento humano, em certos casos é possível observar a perda de habitats marinhos, que consequentemente levam à redução da biodiversidade. Uma faceta visível e atual desta perda de habitats é a morte de corais, que está relacionada com o aumento de temperatura do planeta e a acidificação da água do mar, em parte atribuíveis à ação humana.

Uma das soluções que atualmente é considerada mais promissora para fazer face à perda de habitats é a implementação de recifes artificiais que oferecem abrigo a organismos. Os recifes artificiais são utilizados há muito tempo como parte de estratégias de regeneração de ecossistemas marinhos. No entanto no passado tanto o material constituinte como a geometria ou desenho estrutural não eram alvo de estudos muito detalhados ou apurados, havendo exemplos da reutilização de vários materiais e estruturas tais como carros inutilizados, barcos afundados, pneus usados e outros tipos de resíduos para a implementação de recifes artificiais. Com o desenvolvimento da ciência e o interesse nesta problemática foram desenvolvidos recifes artificiais amigos do ambiente, feitos a partir de materiais não tóxicos. Atualmente a temática associada ao uso dos recifes artificiais continua a ser estudada com enorme interesse. Uma das vertentes mais importante deste estudo foca-se na interação entre as estruturas de recife artificial e o fluxo da água envolvente, que permite analisar o impacto local destas estruturas tanto do ponto de vista ecológico como do ponto de vista da erosão.

Existem várias metodologias que permitem analisar a interação de recifes artificiais com o fluxo de água circundante, algumas delas experimentais tais como a análise do comportamento hidrodinâmico em canal hidráulico associada

a técnicas como a PIV (particle image velocimetry ou Velocimetria por imagem de partículas). Outra abordagem consiste na utilização de ferramentas numéricas, por exemplo por via da utilização de modelos de CFD (computational fluid Dynamics ou dinâmica dos fluidos computacionais). Ambas as metodologias apresentam vantagens e inconvenientes. As metodologias experimentais possibilitam uma visualização direta de resultados, com recurso a instrumentação específica que permite a medição de variáveis essenciais tais como velocidades em determinadas localizações ou perfis de velocidades, pressões, padrões de erosão, entre outras. No entanto normalmente estão associadas a tempos prolongados de execução, tanto pela necessidade de preparação de protótipos à escala como para a realização dos ensaios propriamente ditos. Normalmente também possuem algumas limitações associadas ao espaço disponível, à escala dos protótipos e às condições de ensaio (correntes, ondas, natureza e forma do substrato) que é possível realizar. Por outro lado, os modelos numéricos permitem a simulação das condições próximas das reais e o estudo de geometrias mais complexas. No entanto muitas vezes os modelos gerados são exigentes em termos computacionais, requerendo tempo de preparação e de computação substancial, assim como recursos de hardware significativos. O programa ideal inclui ambas as abordagens, ou seja modelos numéricos que são devidamente calibrados e adaptados a medições realizadas in situ ou em modelos experimentais à escala

A presente dissertação de mestrado, inserida no curso “marine and coastal systems”, pretende contribuir para o estudo do processo de desenho de recifes artificiais, considerando a interação com diferentes cenários hidrodinâmicos. Para alem disso, esta dissertação pretende estudar efeitos particulares que estas estruturas podem ter no meio marinho, incluindo o controlo de efeitos erosivos e a promoção de padrões de corrente atrativos para habitats costeiros. Com esta finalidade, foi feito um estudo inicial da literatura existente, e foram identificados alguns exemplos de desenhos de estruturas de recife artificial. Deste modo, no contexto desta dissertação procedeu-se ao estudo de quatro recifes artificiais (cubic artificial reef, adapted reef ball, upwelling reef and Yfalos modular artificial reef) no ambiente aquático, expostos a velocidades pré-determinadas. Dada a sua importância, foi também analisada a estabilidade de

cada um dos recifes referidos, tendo em vista o estudo das condições adequadas a promover para garantir a estabilidade dos mesmos em ambientes sujeitos a maior agitação. De modo a orientar o estudo realizado nesta dissertação, considerou-se como caso de estudo a aplicação das estratégias estudadas a uma determinada região do Parque Natural do Litoral Norte, em Esposende.

Considerando a importância atual que as ferramentas digitais têm no processo de conceção e fabrico de estruturas mais inovadoras, assim como a possibilidade de integração do processo de desenho com a análise hidrodinâmica e o papel importante que podem ter neste desenho, adotaram-se também ferramentas de desenho paramétrico para a conceção das estruturas de recife artificial complexos. Deste modo, o primeiro passo consistiu na criação dos desenhos das peças de recife artificial em 3D com recurso à ferramenta Rhinoceros®. Foram realizados dois desenhos para cada geometria, um que representa as dimensões reais de cada recife artificial e outro que adota a escala de 1:20 do tamanho real. Os comportamentos hidrodinâmicos das geometrias à escala real foram analisados com recurso à ferramenta numérica Ansys®, enquanto que as geometrias à escala reduzida foram analisadas utilizando a ferramenta REEF3D®. Foram definidas as mesmas condições fronteira para ambos os casos, considerando as condições da área piloto selecionada no Parque Natural do Litoral Norte. Utilizando os mesmos dados, foi ainda realizada a análise da estabilidade de cada recife artificial face às condições da área de estudo adotando um procedimento de interação fluido-estrutura (one way), recorrendo-se para o efeito a um módulo mecânico e a um módulo de fluidos.

Em geral as duas ferramentas numéricas utilizadas apresentaram resultados semelhantes. O *upwelling reef* apresentou uma maior interação com o fluxo de água, enquanto o *Yfalos modular artificial reef* apresentou uma menor perturbação do fluxo de água. Os restantes recifes artificiais demonstraram resultados intermédios relativamente aos anteriores em termos de perturbação do fluxo de água, ainda que todos eles tivessem apresentado particularidades interessantes e apropriadas para aplicações específicas. Relativamente à estabilidade foi observado que, de acordo com os resultados obtidos com a ferramenta Ansys®, o *upwelling reef* propicia as condições para uma maior

estabilidade entre todos os que foram analisados, ao passo que a *adapted reef ball* apresenta uma maior suscetibilidade a instabilização devido ao efeito da velocidade da água e deste modo menor estabilidade, não tendo no entanto atingido o ponto de instabilização. Os restantes recifes artificiais apresentaram comportamentos intermédios relativamente aos anteriormente mencionados.

A título de conclusão geral, para as condições da área de estudo observou-se que geometrias mais próximas da apresentada pelo *upwelling reef* parecem apresentar as melhores condições para garantir a estabilidade das estruturas face ao efeito da velocidade da agua. Adicionalmente, e tendo em vista a sua utilização com o objetivo de promover efeitos de *upwelling*, também a geometria do *upwelling reef* pareceu ser a mais favorável e melhor fonte de inspiração para desenvolvimento de estruturas no futuro. Concluiu-se ainda que a abordagem estudada pode ser muito útil no processo de desenho e conceção de estruturas de recife artificial tendo em vista aplicações especificas, considerando a importância de adequar a geometria aos requisitos de estabilidade, de interação com o fluido envolvente e da regulação de processos erosivos.

Abstract

The current dissertation seeks to improve the scientific knowledge about artificial reefs design, as well as on their impact on the surrounding fluid environment. Furthermore, this dissertation enriches the understanding of different artificial reefs effects on the (potential) biological development, taking in consideration local interactions between them.

This dissertation aims to analyze different artificial reef geometries (cubic artificial re one that represents the real dimensions of each artificial reef and another that adopts a scale of 1:20 of the real size, an adapted reef ball, the upwelling reef and the Yfalos modular artificial reef) impacts on the flow field velocity (based on Exposende natural parck), which might create water velocity patterns beneficial for coastal habitats.

In order to reach the objectives, first it was used the software Rhinoceros to design the chosen artificial reefs, two designs were made for each artificial reef geometry, one that represents the real dimensions of each artificial reef and another that adopts a scale of 1:20 of the real size. The solids were then imported to the Ansys® software (real size geometry) and REEF3D® (1:20 of the real size geometry). The artificial reefs were then submitted to CFD tests, using the boundary conditions based on the Esposende North Littoral Natural (same for all the models regardless the software or size) in order to understand the impact of each artificial reef on the local hydrodynamics. It was also carried out a stability test using the software Ansys® with the same boundary conditions as before.

In general, the two numerical tools presented similar results. The upwelling reef showed a greater impact on the local hydrodynamics, while the Yfalos modular reef presented a lesser disturbance on the local hydrodynamics. The cubic artificial reef and the adapted reef ball presented intermediate impacts on the local hydrodynamics. In terms of stability the upwelling reef presented a greater stability while the adapted reef ball presented the lower stability values (although never reaching instability).

It was concluded that for the present conditions the upwelling reef might be the most viable option (assuming only the chosen artificial reefs) since that it presented the greatest stability among all the solids and promoted the local upwelling and back eddies which are determinant factors for marine habitats.

Key words: Artificial reef, flow field, hydrodynamics, CFD, Design, coastal habitat

Contents

List of Tables

List of Figures

List of equation

List of Abbreviations

ρ- Represent the fluid density

u_i and u_j - Represent the average velocity (Equation 2)

μ - Represent the dynamic viscosity of the fluid

u_i' and u_j' -Represent the fluctuating velocity

$(-\rho u_i' u_j')$- Represent the Reynolds Stresses

p- ~~Rep~~resents the static pressure

μ_t -Represent the turbulent viscosity

u_i -Represent the time-averaged velocity (Equation 3)

δ -Represent the Kronecker delta,

k -Represent the turbulent kinetic energy

$G_k -$ Represents the generation of turbulence kinetic energy due to the mean velocity gradient.

G_b-Represent the generation of turbulence kinetic energy due to buoyancy

Y_M –represents the contribution of the fluctuating dilatation in compressible turbulence to the overall dissipation rate.

a_k and a_ε - Represent the inverse effective Prandtl numbers for k and ε respectively

$S_k$and S_ε are used as source terms

σ_k and σ_ε - Represent the turbulent Prandtl numbers for M and N, respectively.

$C_{1\varepsilon}, C_{2\varepsilon}, C_{3\epsilon}$ -Represent constants

S_k and S_ϵ – Represent user-defined source term.

u – Represent the horizontal velocity

g- Represent the gravity acceleration

k- -Represent the wave number

H- Represent the wave height

w- Represent the frequency

y- Represent the target depth

d-Represent the total depth

AR- Represent artificial reef

MFAR- Represent multifunctional artificial reef

1.Introduction

1.1. Theoretical framework

Coastal areas not only imply to monitor the sea but also land and atmosphere as separate systems, or all of them as one. Therefore, coastal areas are very interesting and challenging places to survey (Simon Haslett, 2016). Coastal areas are very appealing places both to tourism and housing, however the overpopulation near to the coast leads to environmental problems ,such as impacts on the aquatic habitats and water parameters (Simon Haslett, 2016). The main factors causing pressures on the ecosystems can either be related anthropogenic stressors or natural oscillations, or a combination of both (Correia et al., 2015). The human coastal development seems to be linked with habitat loss associated with pollution, differences in the sediment transport and nutrients input (Correia et al., 2015). Anthropogenic impacts over these areas are a major concern in Portugal, as more than half of the population lives near the coast (Ferreira, Dias and Taborda, 2008), which implies the building of large structures. One example of man-made structures are dams which can cause a deficit of sediment reaching the coasts, weakening the coastal sediment nourishment. It is estimated that, in Portugal, around 80% of sediment is lost (Santos et al., 2014).

Over the years different strategies were used to mitigate the anthropogenic impact in the coastal zone, whereas nature based solutions (such as artificial Reefs) present themselves as promising options (Schoonees *et al.*, 2019). Artificial reefs (AR) have been used in the past and nowadays are increasing their popularity due to their multiple applications (Harris,1995). ARs have been placed in shallow waters around the world with a great variety of purposes, from mitigating of land erosion and preserving coasts, protecting habitats, entertaining, fishing, and biotic diversity promotion (Düzbastilar and Şentürk, 2009).

By applying these structures as part of restoration strategies it is possible for coastal managers to customize the original bottom in a better version by altering the physical environmental conditions of an area in order to protect the land from erosion (Harris,1995) and enhance the biological activity. In some cases, the ARs

deflect horizontal ocean currents upwards, inducing the so-called upwelling. Upwelling in general brings the deeper, colder and nutrient rich water to the surface, which in turn stimulates the biological productivity of the surface waters (Harris, 1995).

AR can either be produced from several reef units, or a single larger unit of a certain material. The top of the AR can be underwater (submerged), above the surface of the water (emergent), or shifting between submerged and emergent, according to the tide level and other factors affecting the water level (Harris, 1995).

A The use multifunctional artificial reefs (MFAR) (Maslov *et al.*, 2019) may be considered as a relatively modern approach. In addition to protecting the local beach and increasing the surfing possibilities, these structures are considered to promote the environmental value of the areas where these are built. MFARs are promising instruments for marine ecosystems rehabilitation and may also provide some additional benefits in terms of erosion mitigation. Tourism can also benefit from the installation of this kind of structures (Maslov *et al.*, 2019). In order to improve the resistance and durability of these structures, the design innovation is an important aspect to explore in order to achieve the most appropriate solutions (Maslov *et al.*, 2019).

1.2. Scientifical value

The following dissertation is intended to contribute to the scientifical knowledge about ARs design. Furthermore, it has the intent to help future coastal management plans, since it will include two different approaches to simulate the impact of ARs in a certain type of inflows. Two numerical tools were adopted for this study, using the exact same parameters, but different scales (size), which can be helpful for future discussions.

1.3. Objectives

The current dissertation intends to investigate how different AR shapes impact the local hydrodynamics, as well as how this information can be used to support

the reef structure design. It is also proposed to use computational fluid dynamics (CFD) to analyse the benefits of each design to the local environment.

The tests listed below will be utilized to offer important feedback for future designs and alternative simulation techniques.

Additionally, the differences between a real scale model and a scaled down model will be analysed, in order to assess the possibility to save computational resources when obtaining the required numerical results.

In this study, in order to simplify the problematic, a flatbed (bottom wall) was assumed for all examples. However, this study may be continued in the future by using high resolution topographies of the study area and the production of larger models, so that a coastal management model is implemented, as close as possible to the reality.

1.4. Contextualization

The following dissertation was developed within the context of the research project ASTRIIS - Atlantic Sustainability Through Remote and In-situ Integrated Solutions, with reference POCI-01-0247-FEDER-046092, funded by PT2020-SII&DT - Mobilizadores, and cofunded by FEDER through COMPETE2020, conducted by the University of Minho, in partnership with University of Algarve. The dissertation plan was devised by a multidisciplinary team with different backgrounds.

In the following dissertation two numerical tools were used to simulate the behavior of the fluid when interacting with different ARs geometries. The first numerical tool, Ansys® Fluent, was used to build a real size model. Since the professional license was not available at the time of conducting the numerical experiments, a student version was used which limited maximum number of elements in the mesh. The second numerical tool was REEF3D® (REEF3D, 2022), developed by a team of professors and researchers from NTNU in Norway, was used to develop a scaled model 1:20. The scaling was adopted in order to circumvent the RAM memory requirements of a full-scale model.

In order to simplify the analysis at this stage, a flatbed (bottom wall) and a constant inflow were considered for all models. Biofouling, changes on the geometry due to the water action, shoreline changes, tides, and sediment movement were not taken into consideration. Due to computational limitations and geometry complexities, at this stage only one module of each reef was studied. Furthermore, at this stage no corrections were made in order to account for scale changes by maintaining Reynold’s coefficient and Froude number.

2.State of the Art

2.1. Coastal systems

The coast represents the intersection between oceans, land, and atmosphere, whereas all three contribute to the physical and ecological evolution of coastlines (Haslett, 2008). There are several processes that make the coast so special, such as the upwelling event, which is possible to contemplate in some of the world's coastal systems. The upwelling event is responsible for 20% of the global fish production while occupying less than 1% of the world oceans' surface area (Botsford *et al.*, 2006). Also, some coastal systems have high levels of primary production as a result of fertilization induced by nutrients that come from land (Nixon *et al.*, 2010). These type of processes allow the coastal areas to accommodate a huge variety of marine habitats, so that the major marine biodiversity concentrates near the coast (Gray, 1997). Furthermore the coast is an important economical factor, as these areas tend to be extremely populated and usually represent an attractive zone for tourists and other economic activities to settle (Alves *et al.*, 2015). Contemplating the coastal tourism as an industry that provides recreation services that affects profits, it is crucial to protect the environment and all the facilities that surround it in order to offer to the visitors a nice experience and balanced growth (Alves *et al.*, 2015).

Nowadays it is estimated that more than half of the human population lives near the coast, and often people and nature enter in a conflict of interests (Haslett, 2008).

2.1.1. Upwelling

An upwelling is a phenomenon that happens near to certain coastlines, with the alongshore winds driving the (warmer) surfaces water which are located nearshore, offshore (Largier, 2020). This results in the emerging of the cold and nutrient rich water from the depth into the euphotic zone (near to the surface) (Largier, 2020). High availability of nutrients promotes higher rates of photosynthesis in the euphotic zone, this results in high biological productivity levels in the form of phytoplankton blooms (Largier, 2020). The coastal areas that

are covered by this phenomena usually exhibit a high abundance of marine life, as the phytoplankton is the main driver to support primary and secondary consumers that will be considered prey to larger types of fish, mammals and birds (Largier, 2020).

2.2. Coastal and marine habitats

The ocean incorporates a large part of the world's biodiversity (Gattuso *et al.*, 2018), whereas a huge part of these organisms find their habitat in the coastal systems. The environment satisfaction of marine organisms depend on a number of different requirements like food, shelter, and mating opportunities (Boström and Mattila, 1999). These demands may be altered over time, although food and shelter being considered as the driving factors for habitat choice (Boström and Mattila, 1999). Another critical characteristic which determines a viable habitat is the vegetation in that area, as it provides simultaneously a source of food and protection from predators (Boström and Mattila, 1999).

Nowadays, the worlds coastal habitats are under threat, at high risk of destruction, due to a diversity of factors such as changing weather patterns, pollution, invasive species and overexploitation (Laurance, 2010). Additionally, the growing unsustainable exploitation of fish developed a huge pressure under the global fish stocks, impacting not only the quantity of fish but also the trophic cascades (Wilson *et al.*, 2010).

The climate change also has an influence on the coastal ecosystems, as worldwide temperature rising is expected to provoke thermal anomalies, which have consequences such as the coral bleaching (Wilson *et al.*, 2010). With the bleaching of corals, other types of impacts are expectable, such as loss of shelter of native species (e.g. fish), coral death and non-native species' proliferation (Hoegh-Guldberg et al., 2007).

2.3. Erosion

Many coastal systems around the world face coastal erosion, caused by both natural and anthropogenic activities, whereas it is estimated that coastal erosion

causes a negative impact in about 70% of earth sandy beaches. Waves may be considered one of the most powerful natural forces that act as major players in the coastal development. Whenever waves approach the shoreline, their behaviour is modified due to the shallow water. Frequently is it possible to observe wave refraction, this physical process is responsible for altering the bottom topography by accumulating or removing sediment from the target site, being an important factor in beach erosion (Munk and Traylor, 1947). Sea level rising is one of the most recent problematics which is formerly of natural origin, but its development rate is also influenced by anthropogenic activities. There is an important relationship between sea rising and the erosion of sandy beaches, as rising sea level allow the high energy waves to reach farther up the beaches and transport the sand to offshore and consequently, contribute to lack of sediment on the beach (Leatherman, Zhang and Douglas, 2000).

Whenever sediment supply is not sufficient to assure shoreline maintenance, a landwards movement is triggered, reducing the dune's capacity to absorb energy from storms (Vousdoukas, Almeida and Ferreira, 2012). Coastline retreat generates several undesirable outcomes, such as increased vulnerability of populations and infrastructures (harbours, facilities, coastal tourism infrastructures, houses) to storm surges (Vousdoukas, Almeida and Ferreira, 2012). In Europe, coastal erosion is a major concern whereas it is estimated to cause coastal land loss of around 15 km^2 per year. Annually around 3 billion euros are spent in order to mitigate this issue (Rijn, 2011).

2.4. Artificial Reefs

ARs (AR) are defined as submerged structures which are deliberately placed on the substratum (seabed), in order to mimic some characteristics of natural reefs and are designed to be durable and environmentally friendly, unlike previous underwater ARs which were made out of all types of materials, ranging from tires to sunken ships (Fabio *et al.*, 2019).

Recently, there has been an increase in research on MFARs, these structures are serious aspirants to drastically change coastal management. Previous experiences have proved that these structures may generate ecological, socio-

economic and technical advantages (Fabio *et al.*, 2019). Their main purposes include: (1) restoration and repairing of marine ecosystems in areas damaged by natural and anthropogenic stressors; (2) coastal protection, (3) energy production, (4) support of recreational and (5) sports activities (Fabio *et al.*, 2019).

2.4.1. Promotion of marine habitats

ARs are widely used around the world to improve and protect marine habitats, especially inshore fisheries. Several kinds of ARs were developed for this purpose, with various designs and different types of materials – either materials of natural origin like rocks, or manufactured materials like cement and concrete (Challinor and Hall, 2008).

A substantial amount of evidence is available which indicates that, in particular cases, AR can benefit both the ecology and conservation of the biodiversity, as this structures have the capacity to replace habitats with are otherwise under threat – either due to human activity or environmental changes (Challinor and Hall, 2008). In certain cases these structures even have the ability to convert non-productive areas into productive areas (Challinor and Hall, 2008).

In Japan, ARs are being used for a long time, with the aim to increase the biomass and abundance of target species, such as lobsters and abalone (Challinor and Hall, 2008). It has also been established that whenever the habitat is limited, the deployment of these structures may enhance local stocks and could even provide larval settlement (Challinor and Hall, 2008). In recent studies, it was demonstrated that it is also possible to promote the growth of certain types of benthic macroalgae near to Ars, when all the conditions, such as temperature, are optimal (Sheng, Tang and Wang, 2018).

There are also cases where these structures were used to rehabilitate a target environment. In Salcombe, in 2002, the natural habitats were damaged, so ARs were deployed in order to mitigate the impact and ecosystem loss. It was reported that the structures were being colonized by sponges, sea squirts and cup corals (Challinor and Hall, 2008).

2.4.2. Coastal protection

The use of MFARs for coastal protection has already been explored by several scientists in past. However, nowadays, there is a growing scientific interest in novel multi-functional coastal defence structures with secondary purposes (Evans *et al.*, 2017).

In the Gulf of Mannar, real size ARs with trapezoidal shape were deployed (Jayanthi *et al.*, 2020). The results of this experiment showed that the trapezoidal design provided a reduction of wave impact on the shore, thereby reducing erosion and supporting sediments deposition (Jayanthi *et al.*, 2020).

Another study was carried out in Australia in order to understand the impact of MFARs in a system (da Silva *et al.*, 2020). This study was based on the first ever worldwide deployed MFAR, which aimed at coast protection and surfing enhancement (da Silva *et al.*, 2020). The study analysed twenty years of morphological changes around the reef, as well the reef's impacts on hydrodynamics and wave propagation (da Silva *et al.*, 2020). The results showed an updrift accumulation of sand. The main goal of providing coastal protection was obtained by increasing wave energy dissipation, which lead to the reduction of upper beach erosion (da Silva *et al.*, 2020).

In another study, in India, ARs were deployed in two different locations, to study the evolution of the coastline. The results obtained were compared to of other sites where no deployment was made. After 18 months a significant sediment accumulation was observed in the beaches that were protected by the ARs (Black *et al.*, 2020).

2.4.3. Economic impact

The economy can be a major beneficiary of AR deployments, as these have several advantages, such as enhancing of shoreline protection, fishing resources, recreational fishing and diving opportunities (Pendleton, 2004). ARs have a positive impact in economy, that help to sustain local economies and

provide tax revenues, particularly in areas where scuba diving attracts visitors (Pendleton, 2004).

A study was performed with the aim to calculate the daily average amount that a person would spend visiting ARs in Alabama, Mississippi and Louisiana. It was concluded that the average daily value was 199 dollars per person, making a total annual amount of over 7.4 milion dollars (Pendleton, 2004).

2.4.4. Influence in the environment

Previous knowledge demonstrated that ARs could have an effect on the ecological proliferation (Liua *et al.*, 2013), sometimes due to the interactions between the AR and the flow (Liua *et al.*, 2013). When the AR is deployed in the seabed, eventually near to the reef it will be possible to observe local upwelling, different current fields, and eddy's in the front and/or back of the AR (Liua *et al.*, 2013). When the upwelling is enhanced it is usually possible to observe high values of primary production (Liua et al., 2013). An AR also mimics features of natural reefs such as protecting, concentrating and enhancing populations of marine species (Wang et al., 2018). When deployed, these structures influence the sea bottom available space and change the original topography. These topographic changes make the ARs a different type of approach, because when the topography is changed, the water flow field changes. In these types of scenarios, the water flow field changes to satisfies the objective of the coastal managers. When the flow is separated by the AR blocks, the water flows upwards and downwards (Wang et al., 2018), promoting upwelling. Therefore, it is important and essential before the deployment of any type of AR to study its impacts and effects in laboratory simulations, for example using computational tools, in order to understand how these structurers really impact and alter the local flow.

2.4.4.1 Reef shape and hydrodynamic models

Nowadays much of the research on the area of ARs is focussed on the effect of the reef shapes on local hydrodynamics and flow fields. Scientists that study the effect of the flow field around different types of AR, usually apply different

types of methodologies, some of them are physical like the testing of scaled prototypes in water flumes, and some are based on numerical simulations using mostly CFD. When studying fluid dynamics, it is very important to understand the velocity flow fields, simulating currents from different angles and understanding the interaction of the reef structure with the incoming current.

2.4.4.2. CFD models

CFD is a technique used to solve complex mathematical models of fluid dynamics with computers (Joshi and Ranade, 2003). The purpose of the flow model is to find out how the flow behaves in a given system for a given set of inlet and outlet conditions. These conditions are usually called boundary conditions (Sayma, 2014).

In order to study the water flow behaviour around the AR, CFD is a good alternative at a low cost, so that is been used often (Kim, Jung and Na, 2021), for many different purposes.

The CFD methodology nowadays is very popular in the ARs studies because it is possible to obtain reliable results through the computer, for a low cost, that can give to the user information about the AR design, interaction with fluids, inside, and outside, of the AR (Shen *et al.*, 2020; Wang *et al.*, 2021). The CFD simulations are also a good solution when the user wants to simulate a true scale scenario, while experimental methodologies mostly require either a scaling up or down. In most cases, realistic conditions cannot be economically represented and thus results need to be extrapolated. This problem does not exist when model CFD simulations (Sayma, 2014), being the only model limitation the hardware .

In these types of models, the study of the water flow near to the AR is mainly based on two numerical approaches, the standard k-ε model and the renormalization group RNG k-ε model (Kim, Jung and Na, 2021).

The standard k-ε model is a very popular turbulence model but in certain conditions it performs poorly if large pressure gradients are present (Kim, Jung and Na, 2021). On the other hand, the RNG k-ε model performs better in certain

scenarios, for example when the shear velocity field is more complex and needs to be described by a high stress rate (Kim, Jung and Na, 2021).However, this does not mean that RNG *k-ε* model always shows a better performance than the standard *k-ε* model in terms of analysing the water flow around an AR or a structure (Kim, Jung and Na, 2021). The selection of the most appropriate models depends on the target structure and the water flow conditions (Kim, Jung and Na, 2021).

2.4.4.3. Previous research on CFD topics

The CFD models can have multiple applications, when studying artificial reefs, such as tracking upwelling induced flows by structures and studying how the flow field changes in the presence of solids with different geometries.

In a recent study, the “rotary-shaped reef”, composed by eight rectangular blades and a bottom plate, which forms a semi-open structure, was analysed using CFD (Jiang *et al.*, 2020). In this article the effect of different holes and diameters were analysed using CFD. In the experiment the authors found no clear relationship between the “cut-opening ratio” and the flow field effect for that specific structure (Jiang *et al.*, 2020).

Also, in another study the function of “guide plates” was analysed in upwelling formation using CFD analysis (Jiang *et al.*, 2016). In this experiment a cubic frame AR with guide plates was analysed. In the study several simulations were performed and at each simulation the guide plates adopted a different angle. A cubic reef with no plates was adopted as a reference (Jiang *et al.*, 2016). It was concluded that the guide plates can have an impact on the flow field. The installation of angles in the guide plate, in the direction of the inflow, has a significant impact on the flow field, and a smaller or larger angle, such as 30º or 150º can contribute to the upwelling formation (Jiang *et al.*, 2016).

Also, studied by other authors, three previously sunken structures were modelled on a CFD software with the objective of understanding their impact on local environment , where the conditions adopted were based on Malaysia environments (Rahman *et al.*, 2021). The structures that were used were three

legged platforms, located at water depths between 28 m and 80 m below the mean sea level. The structures had different heights and widths (Rahman *et al.*, 2021). The results of the CFD analysis showed that the upwelling was generated by the sunk platforms, and it was also possible to observe the generation of back eddies in the area.

2.5 Previous artificial reefs deployments

The deployment of an AR can be beneficial to the environment if it is well planned. In previous cases the same AR model was deployed in multiple locations (including in different countries), and the results were completely different.

The Reef ball™ is an example of an AR, which was patented in 1996 (Barber and Barber, 1996). This structure was initially developed to enhance the local ecology (Arnouil, 2008). Although with time this structure started to be used for other purposes like shoreline stabilization, oyster growth, mangrove rehabilitation, and as marine protection (Arnouil, 2008). According to previous reports, the reef ball is also used to mimic natural reef features, providing substrate for benthic organisms, such as corals, giving them a surface to attach so that they can grow (Meesters, Smith and Becking, 2015). However, depending on the environmental conditions, the results can vary, as shown by the two following examples where Reef ball units were deployed in different sites.

In the first case, several units of the Reef ball™ were deployed on the Caribbean shore, Dominican Republic, with the aim of acting as a breakwater. The Reef Ball ™ units that were deployed proved to be an efficient solution for shoreline stabilization between 1998 and 2001, considering that the sand volume on the beaches where the Reef Ball ™ were placed, has increased (Harris, 2006). It was also observed that the Reef Ball ™ provided habitat for marine life and proved to be a good substrate for coral growth (Harris, 2006).

On the other hand, when Reef Ball ™ units were deployed at five different observation points at Talang Talang Island, in Malaysia, the study observed that the Reef Ball ™ units ended up being covered mainly by sand, rocks and algae

(Awang and Pit, 2003), after two year period, therefore not having any significant positive impact on the environment.

These types of situations can be anticipated when physical or computational tests are performed before designing and deploying an AR or any type of structure which might impact the local environment.

3.Computational analysis of the interaction between artificial reefs structures and the fluid (software exploration).

In order to complete the objectives mentioned previously, initially three different numerical tools were tested, in order to determine which alternative is more appropriate for analyzing the fluid interaction with ARs.

3.1. Autodesk CFD

The first step to initiate this dissertation was to test a software for the models development. The first attempt was made with the software package Autodesk® CFD. Autodesk CFD is used by engineers to simulate how liquids and gases behave using CFD simulation software (Autodesck, 2022). This software was mainly chosen due to being “user-friendly” and presenting a wide range of applications. However, after running some trial experiments, for the current problematic it was concluded that some limitations would difficult its use for the models under the chosen conditions.

3.2. Ansys Fluent

After performing a literature review it was observed that Ansys® Fluent is the most widely used software for the analysis of the interaction between AR and fluids.

Ansys® Fluent is a fluid simulation software recognized for its sophisticated physics modelling capabilities and industrial leading accuracy. Also, this software is a reliable source of results, since it has been tested and validated in a wide

range of applications. With this numerical tool it is possible for the user to create an advanced physical model and analyze the fluid behavior (Ansys, 2021). It also allows further analysis, by coupling the fluid analysis with subsequent solids analysis including mechanical modeling. Ansys® Fluent allows the user to solve the Reynold's average Navier stokes equation with a variety of equations such as the standard *k-ε model, RNG k-ε model and k-ω model. In this particular case it was used the RNG k-ε model.*

For the above-mentioned reasons, this software package was selected to conduct the study in the scope of this dissertation, in order to determine its interest in the study of the effects of AR on water flow before it is deployed, as well as with helping on the management and planning of each deployment.

3.3. REEF3D

After performing literature review on other types of models which can give more information to the user, REEF3D® presented a huge potential in coastal management and planning. REEF3D® software is still being upgraded, although, it allows the users to study the fluid behavior (currents and waves) and sediment movement in a wide diversity of boundary conditions, including coastal and offshore.

REEF3D® is an open source CFD code (written in an object-oriented C++ structure which allows a flexible design). In time several applications were developed for REEF3D®, including the interaction of waves with obstacles, as well as vegetation impact on coastal protection (Wang, 2020).

3.4. Section conclusions

After an initial stage of first contact and testing, which included generating and analyzing a significant number of models with all the software packages mentioned above, it was decided to focus the research on two computational tools. Ansys® software was selected after obtaining satisfactory results in trials, added to the fact that Ansys® represents the benchmark CFD software for fluid interaction with ARs, according to the literature review performed. The second

software selected was REEF3D®, due to the fact that it represents a promising alternative for physical tests including the simulation of waves, fluid velocity and sediment transport, that could be beneficial for future projects. Based on the literature review, the Autodesk CFD was not so popular in this regard.

4.Study area

In order to test the methodologies adopted, two main study areas were selected as possible application sites- Praia de Faro which is in the south coast of Portugal and Esposende which is located in the northwest coast of Portugal. Both locations are interesting in terms of coastal management: Esposende entails a marine protected area which is currently under study for the future implementation of management strategies, and the south coast due to its biological activity and littoral dynamics. Eventually, due to the time schedule restrictions, only one of the locations was considered.

4.1. Description of the Littoral North Natural Park (LNNP) in Esposende

The study area that was chosen for this dissertation project was the Littoral North Natural Park in Esposende (Figure 1), due to the project in which this dissertation is inserted.

Esposende has a coastline of approximately 16 km with a transition of characteristics between the sandy beach to pebbly beach, rocky outcrops, with the presence of sandy dunes at the backshore (Garcin et al., 2011). Esposende is a highly touristic area, where the population increases significantly during the touristic season. The population average is 427 inhabitant/km2. The main economic activities in the area include tourism, agriculture and fisheries. In recent years this region has been showing coastal erosion problems including coastline retreat, beach profile change, destruction of sandy beaches and dunes, land loss and building and infrastructure damage (Garcin et al., 2011).

The littoral Esposende protected area, was created in 1987, and in 2005 it was reclassified as the natural park of the northern littoral in order to conserve the natural, aesthetic, landscape and cultural values of the area, by the Portuguese law (Decreto Regulamentar nº 6/2005, de 21 de Julho) (Gomes, 2010).

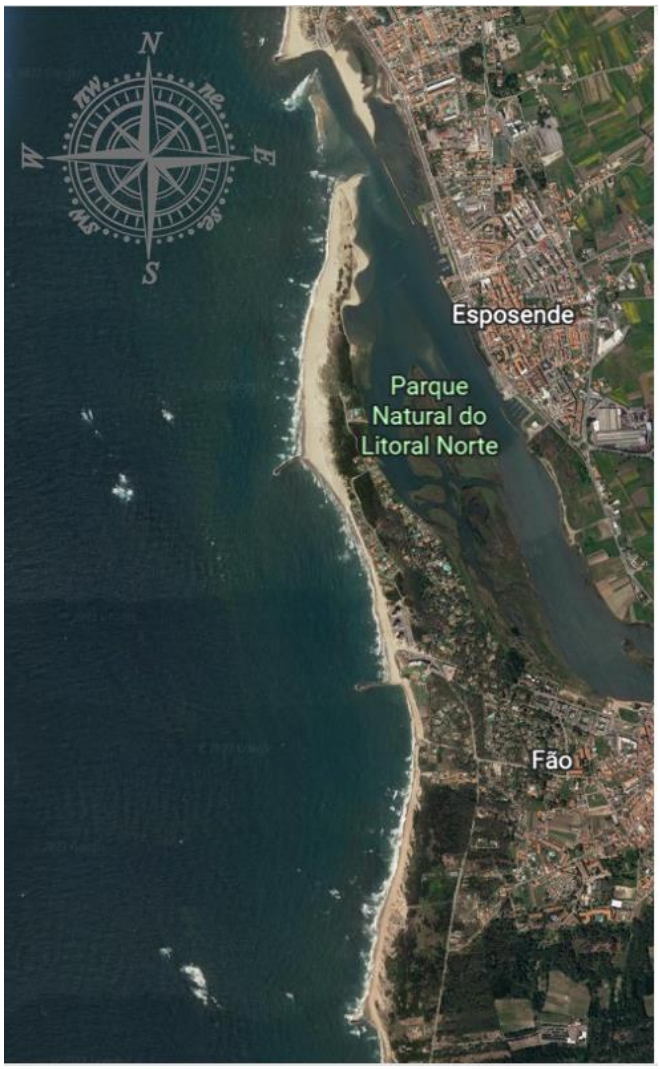

Figure 1-Representation of the study area image adapted from (Google, 2020).

With the objective to contribute to a sustainable coastal management plan, using ARs, it was developed a numerical model, which represents the potential of different ARs geometries, and associate them to different hydrodynamics. Numerical models allow the coastal manager to mitigate the negative impacts, by observing the structure impacts before any deployment.

In the study area, according to previous report's, the tidal system is dominated by a mesotidal regime, with an average neap tide of 1m and an average spring tide of 2.8m (Granja, Monteiro Rodrigues and Danielsen, 2016).

According to previous reports the sediment in the Esposende margin was described as 42% of gravel, 19% of very coarse sand, 12% of coarse sand, 7%

of medium size sand, 4% of fine sand, 11% of very fine sand and 3% of silt (Carvalho and Santos, 2013).

In terms of biological activity, it was reported that in Esposende it is possible to observe a huge variety of organisms, from shrimps small to medium sized and large fish (Carvalho and Santos, 2013).

4.1.1 Data collection and treatment

In order to reproduce the local wave effects on the hydrodynamics in the study area, after a search in the literature the data source adopted was the one made available by the web-site *Puertos del Estado*. This web-site offers information regarding the coastal zone of the Iberian Peninsula, with data available very close to the study area. The *Puertos del Estado* offers: (1) forecast data, (2) real time data and (3) historical data (Puertos del Estado, 2022).

The *Puertos del estado* information is based on sensors spread along the Spanish coastal area, and this information supports a numerical model that is calibrated with in situ data (Puertos del Estado, 2022).

The information used in this study corresponds to the coordinates 9.00ºW; 41.50ºN (closest site to the study area). The historical data based on the numerical model was downloaded, which included the most common wave height per month (significant wave height per month) considering the time frame between 1958 and 2021.

Afterwards, the information was analyzed and four main ‘waves’ were identified, including the highest significant wave, the lowest significant wave, the average height significant waves and the most common significant wave since 1958. The chosen waves are represented in the Table 1.

Table 1-Waves that will be studied based on (Puertos del Estado, 2022).

	Wave height (m)	Wave period (s)	Year of observation	Month of observation
MAX	10.65	15.38	1986	2
Average	4.5	11.24	1971	11
MIN	1.76	11.24	1981	11
Most frequent	3.58	11.76	1969	9

Subsequently, with the objective of obtaining the horizontal velocity of the water particles induced by each wave, the Equation 1 was used (Chakrabarti, 2005; Fabio *et al.*, 2019) . The velocities were obtained using Equation 1 at the moment "zero" (wave crest), where the horizontal velocity is maximum. The depth of the area was not mentioned on the website, so it was assumed a depth of -20m for the following processes.

$$u = \frac{\mathrm{gkH}}{2w} \frac{\cosh k(y+d)}{\cosh kd} \cos(kx - wt)$$

Equation 1-Horizontal velocity of water particles(Chakrabarti, 2005) .

4.1.2. Data results

Table 2 shows the results obtained after applying Equation 1 and using the input values presented in Table 1. When analyzing the results it is possible to observe that the higher the wave height, the stronger the induced velocity in the water particles. These results will be used to support the definition of the boundary conditions to the models that will be addressed in the following chapters.

Table 2-Representation of the inlet velocity corresponding to each wave.

Wave	Height, h (m)	Period, T (s)	Inlet velocity (m/s) (obtained at depth of 20 m)
MAX	10.6	15.3	1.9
Average	4.5	11.2	0.88
MIN	1.7	11.2	0.33
Most frequent	3.5	11.7	0.7

4.2. Possible deployment location

This dissertation is part of a larger project, which aims to deploy an AR unit in the study area (LNNP) Esposende. There are two potential deployment sites represented at Figure 2. The site 1 (-8.12W,41.56N) is chosen due to a wide valley, easy to find, well protected from the dominant incoming wave (west direction), also the sides of this location are dominated by rocky reefs. The site two (-8.82W,41.56N), Although it is more exposed to the incoming waves, have several pre colonized rocky reefs which might promote a better colonization. It is expected to continue the current study, to determine which of the following sites provides the most benefit to the local marine ecology.

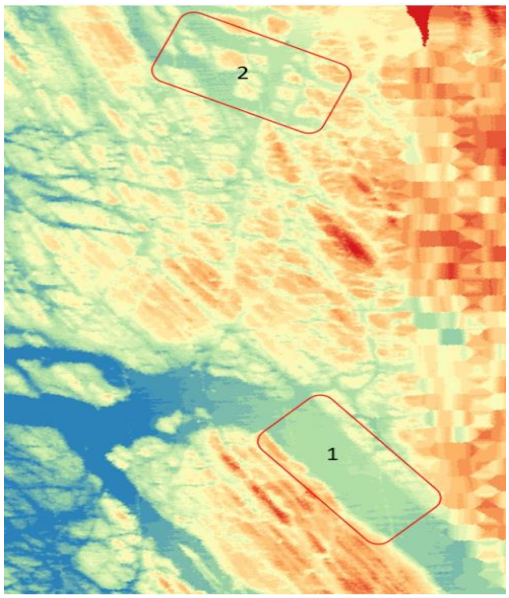

Figure 2-Representation of the possible AR deployment sites.

5. Methodology

This chapter describes the steps taken to assess the different aspects of the interaction between different AR structures and the surrounding fluid. In a first stage, the work conducted was dedicated to validate the first models produced, by comparing the results obtained with the ones found in the literature for similar problems. This first approach is important to validate the methodologies adopted and the reliability of the models produced with the chosen software.

A real-size flow field simulation model was created using the Ansys® Fluent software, as well as a scaled model using the program REEF3D®. In the case of the REEF3D®, a 1:20 scaled model was implemented due to hardware limitations. REEF3D® is intensive in the use of RAM memory, therefore the existing platform showed some limitations for large models.

5.1. Numerical modelling validation

In order to validate the procedures adopted to model the hydrodynamic behaviour of the studied AR units with Ansys® Fluent and REEF3D®, a preliminary validation procedure was performed taking as reference the results reported in the literature by other authors (Wang *et al.*, 2018).

For the validation process, the “case study 36” referred by the authors was chosen. The first step of the validation procedure consisted of designing a reef model with the same characteristics. The model was developed in the software package Rhinoceros 3D® (Rhino), and the model size was the same as the one adopted by the authors(150mm × 150mm × 150mm) (Wang *et al.*, 2018).

After obtaining the reef model a computational domain with the same dimensions as the ones adopted in the previously mentioned publication were adopted (4m × 1.2m × 1m), using the Ansys® tool Space claim. In the case of the REEF3D®, the data related to the definition of the study domain is defined using a .txt file containing all the controls necessary to defining the domain and mesh.

The next step was the creation of the mesh. In (Wang *et al.*, 2018) the “total number of nodes and elements were approximately 1.07×10^6 and 5.25×10^6, respectively. This mesh quality in a software package like Ansys® demands a full license, so in this case it was used a mesh of 43842 nodes and 220112 elements. In the REEF3D® software, the meshing system is automatic, where it is only necessary to choose the cell size of the mesh. A cell size of 5mm was chosen (smallest cell size possible to generate), later a mesh with 848000 cells was generated.

The last step before running the calculations included defining the boundary conditions and the procedure to adopt for solving the flow equations. The equation that was used in this case was the standard k-ε equation, that defines the turbulent intensity of the entire domain (Wang *et al.*, 2018). The boundary conditions that were applied in this case were:

a) Inlet was applied at the front of the domain, which represents the entrance of the computational domain with an inlet velocity of 0.2m/s.

b) Outflow was defined at the back side of the domain, with pressure equal to zero.

c) Bottom wall of the domain was defined as a stationary no-slip wall boundary.

d) The top wall was defined as a moving no-slip wall boundary, the free surface of fluid, with a zero-shear stress and the same velocity as the inflow.

5.2. Reef design

The ARs designs were made using the computer software Rhinoceros®. This Commercial software is commonly used to produce 3D models (Lee and Song, 2021). Rhino is an interesting program in terms of research and industry given its capabilities to reproduce complex geometric shapes (Lee and Song, 2021). It is also very frequently associated to Grasshopper® for parametric design.

Two solids were made for each AR geometry, one using a real scale (analysed in Ansys® software), the other using a scale 1/20 (analysed in REEF3D® software).

5.2.1. Cubic artificial reef

The cubic AR was the first to be developed. It represents a simple hollow cube with holes, without top and bottom plate. Figure 3 shows the rendering of the cubic AR that was inspired by past articles (Jiang *et al.*, 2010; Wang *et al.*, 2018). The dimensions of the real size model are 3m × 3m × 3m (length × width × height) (Figure 4a)). The reduced 1/20 scale solid was 150mm X 150mm X 150mm respectively (Figure 4 b)).

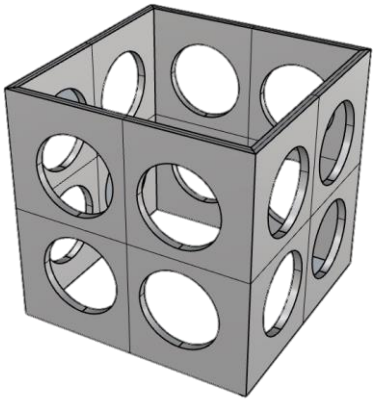

Figure 3-Representation of the cubic artificial reef

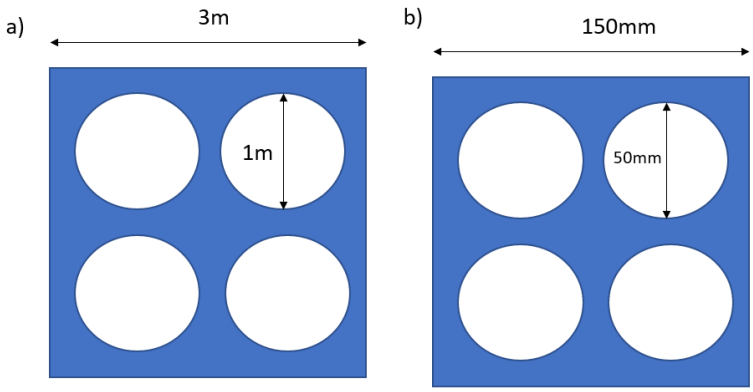

Figure 4-Cubic AR side view a) representation of the cubic AR real size b) representation of the cubic AR scale 1/20.

5.2.2. Adapted reef ball

An adapted reef ball was also studied and modelled, as shown in Figure 5, inspired by the first Reef Ball ™ (Barber and Barber, 1996). The geometry was considered to be uncovered at the top, presenting a larger size circular hole on the top. As before, two geometries were generated, one with the real size, presenting a base diameter of 1.02m, a hight of 0.5m and a top hole with 0.48m of diameter. The other geometry was produced at 1/20 of the original size, presenting a base diameter of 51mm, a height of 25mm and a top-hole diameter of 24mm, as shown in Figure 6.

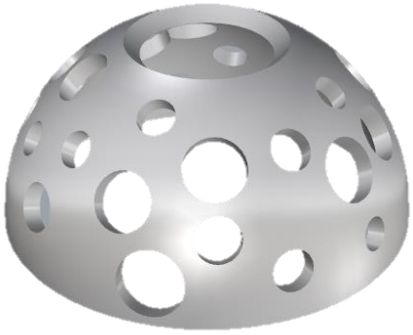

Figure 5-Representation of the adapted reef ball

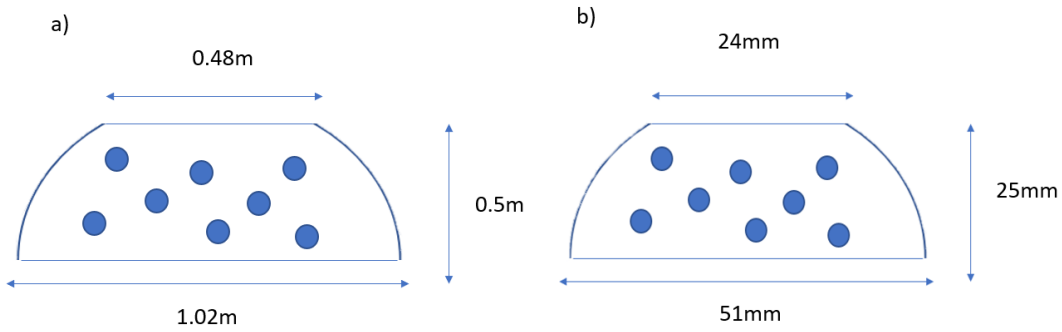

Figure 6-Side view of the AR based on the Reef Ball: a) Representation of the real scale geometry b) representation of the geometry with 1/20 of the size.

5.2.3. Upwelling reef

A relatively new AR design was also studied, the *upwelling reef*, as represented in Figure 7. This design was chosen due to its multifunctionality, aimed at serving as habitat for marine life and upwelling enhancing under the conditions adopted in recent studies (Jiang, Liang and Tang, 2019).

According to the description by the authors in previous studies (Zhang *et al.*, 2021), where the geometry of the *upwelling reef* was described carefully, the dimensions of the original structures were carefully replicated. An original size cube with a width, length and height of 3m × 3m × 3m was created, with a pyramid inside measuring 2.4m at the base and 2.7m at the side edge. A 1/20 scaled geometry was also created, with a cube of 150mm × 150mm × 150mm and a pyramid with 120mm of base and 135mm of side edges, as shown in Figure 8.

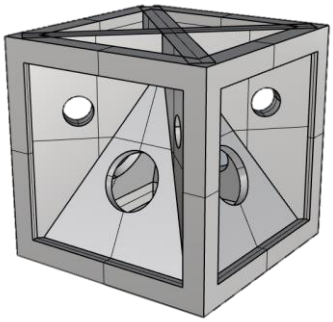

Figure 7-Representation of the Upwelling reef

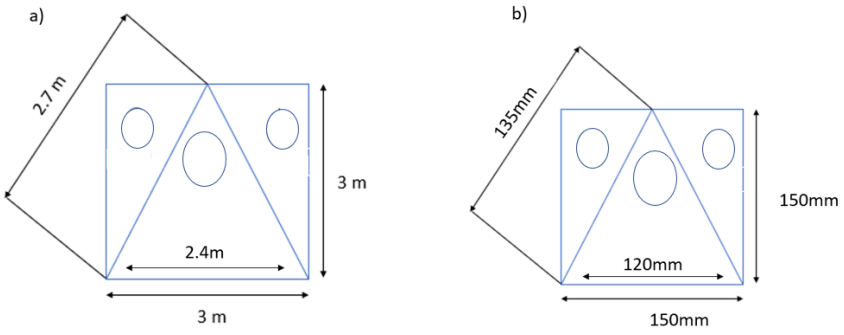

Figure 8-–Upwelling reef side view: a) representation of the real size upwelling reef model b) representation of the 1/20 size of the upwelling reef model.

5.2.4. Yfalos modular artificial reef

The last AR examined was based on the concept by (Designboom, 2021). The Yfalos modular AR is made of several units, which can have different configurations and sizes (Designboom, 2021). In the present study the configuration selected is shown in Figure 9. The information available on previous tests conducted with this structure is scarce since it was first presented on September 23,2021 (Designboom, 2021). This AR was chosen due to its peculiar geometry and promising features, in order to compare its performance with other types of ARs.

A single piece was assumed to have a height of 0.776m, a width of 0.27m and a length of 1.5m, as represented in Figure 10. The arrangement is represented in Figure 11 a) as a real size and at Figure 11 b) at 1/20 of the real scale.

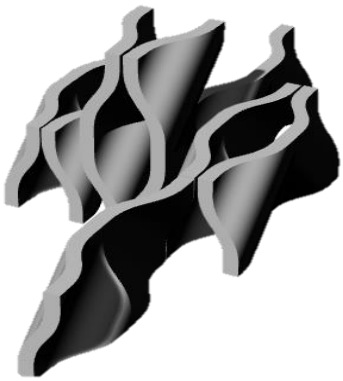

Figure 9-Representation of the Yfalos modular AR, with the chosen configuration (Designboom, 2021).

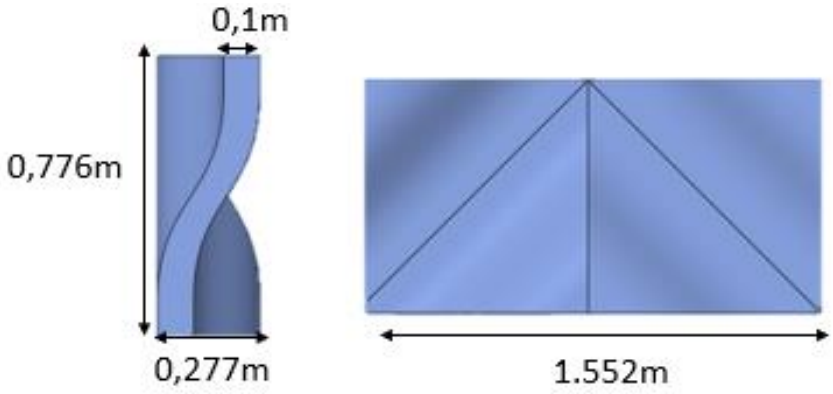

Figure 10- Representation of one real size piece with the assumed dimensions.

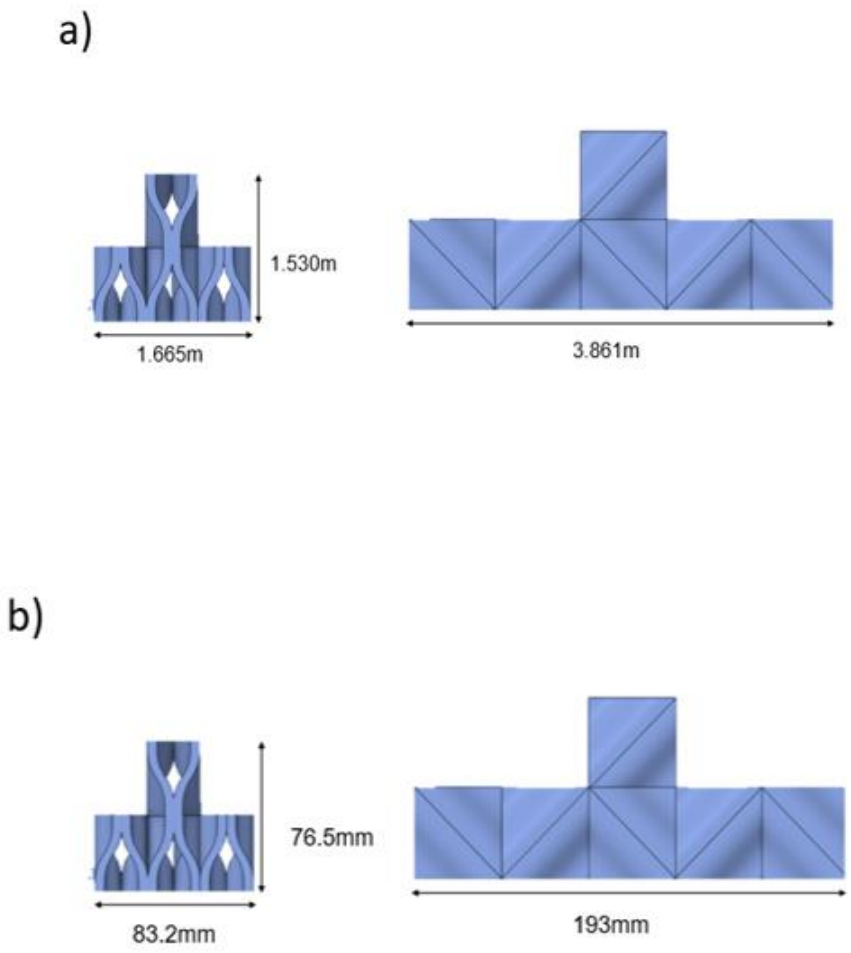

Figure 11-Representation of the modules configuration: a) real scale, b) 1/20 scale.

5.3. Computational domain

The computational domain in a CFD study is the volumetric space where the CFD simulation solution is conducted, which should be considered as sufficiently large to include all the localized and discontinuous processes (Idealsimulations, 2021).CFD simulations require a computational domain that represents a volume of sufficient dimensions around a geometry of interest, which is often represented as a basic box that surrounds the target shape. This approach provides for a straightforward formulation of the boundary conditions (Idealsimulations, 2021).

When utilizing CFD, it is useful to know the body effects on the surrounding flow field before establishing a definitive domain size (Idealsimulations, 2021).

This type of information can be obtain by a preliminary CFD simulation of the target geometry with an oversized domain (Idealsimulations, 2021).

In this study, a preliminary test was dedicated to analyzing the AR effect on the target flow with a large computational domain. The results obtained allowed to decide how large the domain needed to be, in order to achieve an optimal view around each AR.

Each computational domain size has approximately three times the length of the AR after the inlet or inflow, and seven times the length of the AR after it, three times the height (above the solid), three times the width to the right and three times the width to the left, as show in Figure 12 and Figure 13.

Again, for each solid two computational domains were generated, being one for real size models and the other for 1/20 of the size models, the dimensions of those computational domains are represented at Table 2.

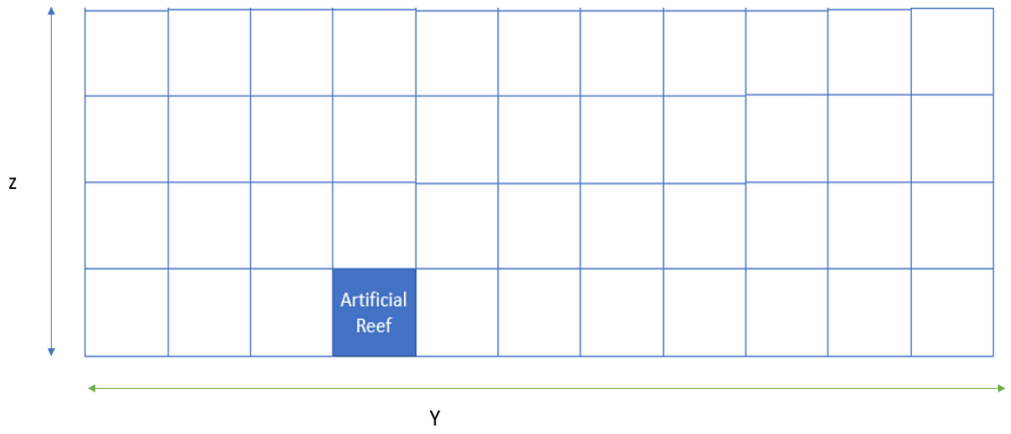

Figure 12- Illustration of the AR domain (Y and Z view).

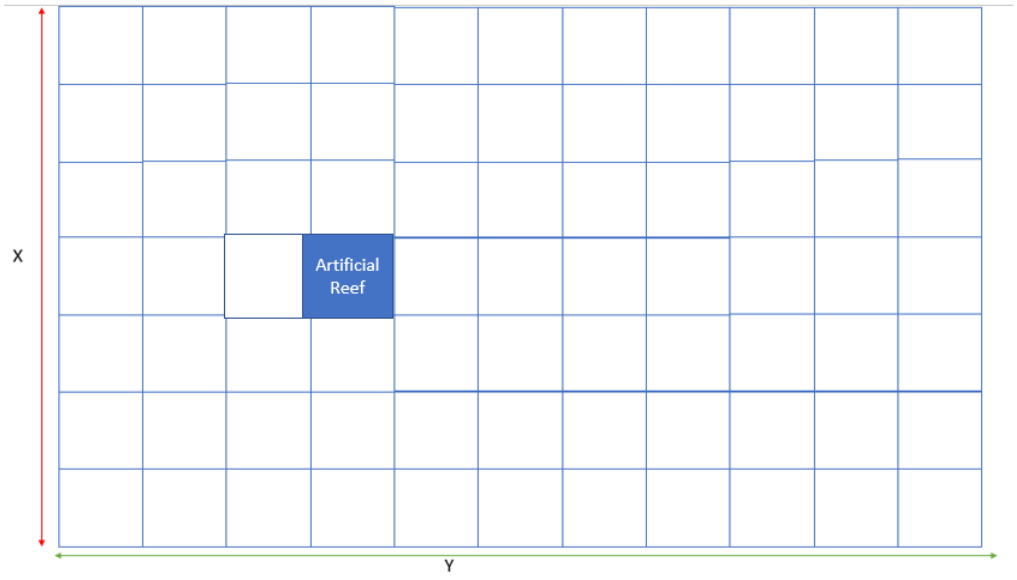

Figure 13- Illustration of the AR domain (X and Y view).

Table 3- Representation of the computational domain sizes.

Solid	scale	Width (m)	Length (m)	Height (m)
Cubic AR	1/1	19	33	12
Cubic AR	1/20	0.95	1.65	0.6
Adapted reef ball	1/1	7.1	11.2	2
Adapted reef ball	1/20	0.35	0.56	0.1
Upwelling reef	1/1	19	33	12
Upwelling reef	1/20	0.95	1.65	0.6
Yfalos modular AR	1/1	11.2	41	6.4
Yfalos modular AR	1/20	0.56	2.05	0.32

5.4. Meshing

After the solid and the domain are set, it is possible to continue to one of the most important processes of the simulation, the domain discretization. This process is the translation of the geometrical and mathematical model variables into numbers (Sadrehaghighi, 2020). Since the user discretizes both the solid body and the domain, generating a set of points called the grid or mesh (Sadrehaghighi, 2020).

The CFD results accuracy have a huge dependence on the mesh parameters such as spacing around the leading edge, fine orthogonality and skewness factors, smooth spacing variation, and a reasonable number of nodes (Sadrehaghighi, 2020).

The meshes for the real size models were generated using the program Ansys® Fluent, while the scaled models mesh was generated using the REEF3D® meshing system.

The models generated with the program Ansys® were limited on the mesh quality, since the student version of the program was limiting the number of elements available. Meanwhile the REEF3D® meshing system only depended on the computer hardware. The final mesh characteristics for the models that were generated in the program Ansys® Fluent are presented in Table 4, while the mesh parameters obtained for the scaled models created with REEF3D® are presented in Table 5.

Table 4- Mesh characteristics of the models that were generated in the program Ansys®.

Solid (real size)	Number of cells	Cell size (m)
Cubic AR	272105	0.5
Adapted reef ball	366248	0.2
Upwelling reef	297405	0.5

Yfalos modular AR	399744	0.7

Table 5- Mesh characteristics of the scaled models that were made in REEF3D®.

Solid (1/20 of real size)	Number of cells	Cell size (m)
Cubic AR	462000	0.015
Adapted reef ball	8510	0.015
Upwelling reef	462000	0.015
Yfalos modular AR	702810	0.015

5.5. Numerical modelling

For all simulations the water density (specific gravity) was assumed equal to 1025 kg/m3 and the fluid viscosity equal to 0.001003 kg/ (m s).

5.5.1. Ansys® models

The water present on every flow analysis was assumed to be incompressible. Factors like the heat exchange were ignored. With the objective to execute the computations, some equations were used by the program, such as the continuity equation(Equation 2), and the Reynolds-averaged Navier-Stokes equation or RANS (Equation 3) (ANSYS.inc, 2013). Both of these equations (Equation 2 and Equation 3) were used to calculate the velocity of the water particles in the present study.

$$\frac{\partial \rho}{\partial t} + \frac{\partial}{\partial x_i}(\rho u_i) = 0$$

Equation 2- The continuity equation (ANSYS.inc, 2013).

$$\frac{\partial}{\partial t}(\rho u_i) + \frac{\partial}{\partial x_j}(\rho u_i u_j) = -\frac{\partial p}{\partial x_i} + \frac{\partial}{\partial x_j}\left[\mu\left(\frac{\partial u_i}{\partial x_j} + \frac{\partial u_j}{\partial x_i} - \frac{2}{3}\delta_{ij}\frac{\partial u_l}{\partial x_l}\right)\right] + \frac{\partial}{\partial x_j}(\overline{-\rho u_i' u_j'})$$

Equation 3- Reynolds-averaged Navier-Stokes or RANS equation (ANSYS.inc, 2013).

Then with the objective to properly model the Reynolds Stresses, the Boussinesq hypothesis was adopted (Equation 4), to relate the Reynolds stresses to the mean velocity gradients (ANSYS.inc, 2013).

$$-\overline{\rho u_i' u_j'} = u_t\left(\frac{\partial u_i}{\partial x_i} + \frac{\partial u_j}{\partial x_i}\right) - \frac{2}{3}\left(\rho k + \mu_t \frac{\partial u_i}{\partial x_i}\right)\delta_{ij}$$

Equation 4- Boussinesq eddy viscosity approach(ANSYS.inc, 2013).

Based on the hypothesis presented on Equation 4, the decisive point to calculate the turbulent motion is the determination of μ_t. In order to calculate μ_t to close the equation, Equation 5 was employed where C_μ= 0.0845 (ANSYS.inc, 2013).

$$\mu_t = \rho C_\mu \frac{k^2}{\varepsilon}$$

Equation 5- Coefficient μ_t (ANSYS.inc, 2013).

Finally, to complete the Equation 4 only two values are missing, the k and the ε that can be obtain using RNG k-$\boldsymbol{\varepsilon}$ model (Equation 6). This model is similar to the standard k-$\boldsymbol{\varepsilon}$ model, although the RNG theory includes several refinements that are not present in the k-$\boldsymbol{\varepsilon}$ model (ANSYS.inc, 2013).These features make the RNG k-$\boldsymbol{\varepsilon}$ model more accurate and reliable for a wider class of flows than the standard k-$\boldsymbol{\varepsilon}$ model (ANSYS.inc, 2013).

$$\frac{\partial}{\partial t}(\rho k) + \frac{\partial}{\partial x_i}(\rho k u_i) = \frac{\partial}{\partial x_j}\left(a_k \mu_{eff} \frac{\partial k}{\partial x_j}\right) + G_k + G_b - \rho\varepsilon - Y_M + S_k$$

$$\frac{\partial}{\partial t}(\rho\varepsilon) + \frac{\partial}{\partial x_i}(\rho\varepsilon u_i) = \frac{\partial}{\partial x_i}\left(a_\varepsilon \mu_{eff} \frac{\partial \varepsilon}{\partial x_j}\right) + C1_\varepsilon \frac{\varepsilon}{k}(G_k + C_{3\varepsilon} + G_b) - C_{2\varepsilon\rho}\frac{\varepsilon^2}{k} - R_\varepsilon + S_\varepsilon$$

Equation 6-RNG k-ε equation (ANSYS.inc, 2013).

5.5.2. REEF3D® models

In the present case study, a CFD module was used in all the simulations, where the incompressible Reynolds-averaged Navier-Stokes (RANS) equations was used simultaneously with the continuity equation to solve the fluid flow (Equation 1 and 2) (Kamath *et al.*, 2015). In order to define the turbulence model for the computational domain, the standard k-***ε*** model was used (Bihs, 2021) represented in Equation 7.

$$\frac{\partial}{\partial t}(\rho k) + \frac{\partial}{\partial x_i}(\rho k u_i) = \frac{\partial}{\partial x_j}\left[\left(\mu + \frac{\mu_t}{\sigma_k}\right)\frac{\partial k}{\partial x_j}\right] + G_k + G_b - \rho\varepsilon - Y_M + S_k$$

$$\frac{\partial}{\partial t}(\rho\varepsilon) + \frac{\partial}{\partial x_i}(\rho\varepsilon u_i) = \frac{\partial}{\partial x_i}\left[\left(\mu + \frac{\mu_t}{\sigma_\varepsilon}\right)\frac{\partial \varepsilon}{\partial x_j}\right] + C1_\varepsilon \frac{\varepsilon}{k}(G_k + C_{3\varepsilon} + G_b) - C_{2\varepsilon\rho}\frac{\varepsilon^2}{k} + S_\varepsilon$$

Equation 7-Standard k-ε equation (ANSYS.inc, 2013).

5.6 Boundary conditions

The boundary conditions were defined inspired in previous studies (Wang *et al.*, 2018). Figure 14 shows a visual representation of the boundaries of the computational domain, the conditions of each boundary were defined as follows:

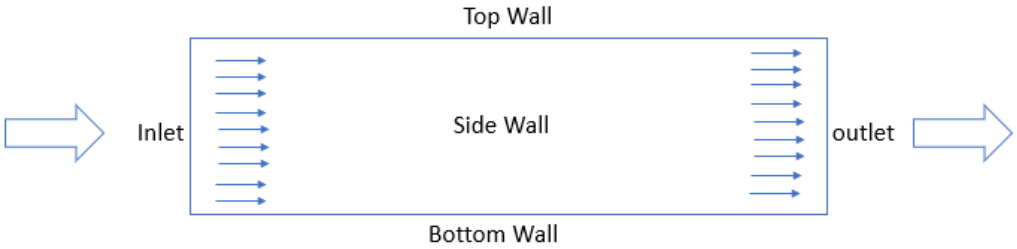

Figure 14- Representation of the boundary conditions of the domain.

a) Inlet/inflow- The inlet conditions consisted of an entrance velocity based on the results of the horizontal velocities.

b) Side walls- the side walls were defined as moving walls, having the same velocity as the inlet.

c) Bottom wall- the bottom was defined as a stationary wall.

d) Top wall- The top wall was defined as a moving wall, with the same velocity as the inlet.

5.7. Stability analysis

This section is dedicated to the study of the stability of each solid regarding the water particle velocity induced by each type of wave, considering the potential overturning of the structure when in the presence of high flow velocities. The stability analysis was conducted using Ansys® static structural. In these steps it was assumed that all the structures were made out of concrete with a density of 2200 kg/m^3.Also it was assumed that the standard earth gravity force is 9.8066 m/s^2. In this step the real size ARs were used.

The first step to assess the stability of the reef structure consisted on importing the flow pressures obtained from the analysis of Ansys® Fluent to the Ansys® static structural analysis module. Typically, this type of analysis is called a one-way Fluid Structure Interaction analysis. Subsequently, another mesh was defined to the AR (only the cube), in this case appropriate to conduct the mechanical analysis. Essentially the flow pressures acting in the structure, which result from the Ansys® Fluent analysis, constitute the action in the struture on the

second Ansys® static structural analysis tool. This mesh was made of 1477 elements and 5242 nodes.

5.7.1. Cubic artificial reef stability test

In a subsequent stage, four displacement points were added to each corner of the structure supporting plate and prescribed with a displacement restriction, as shown in Figure 15. Then in each of these displacement points, a force reaction probe was placed in order to observe the reaction forces generated on each point. Considering that the AR structures are simply laid on the bottom of the sea, no negative reaction forces are admissible, therefore their occurrence in a simulation means immediate loss of stability.

Finally, four models were made, one for each inlet velocity corresponding to each of the test waves studied,

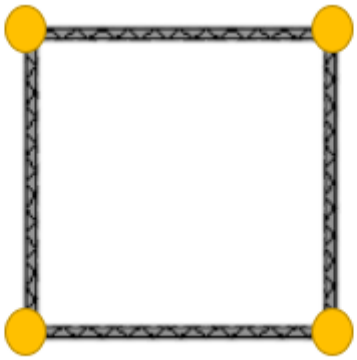

Figure 15- Cubic AR restrained displacement points at the bottom.

5.7.2. Adapted reef ball stability test

In the case of the *adapted reef ball*, the Fluent models were also imported into the static structural tool, and the same procedures were followed as in the previous case. Afterwards the mesh was defined for the *adapted reef ball*, with 5603 nodes and 2228 elements.

Due to the absence of edges in the bottom geometry, two displacement restrictions were defined on the *adapted reef ball* base, as shown in Figure 16.

Then, as before, at each displacement point a reaction force probe was placed in order to observe the loads at each point.

As before, four stability models were performed for each AR, one for each wave data.

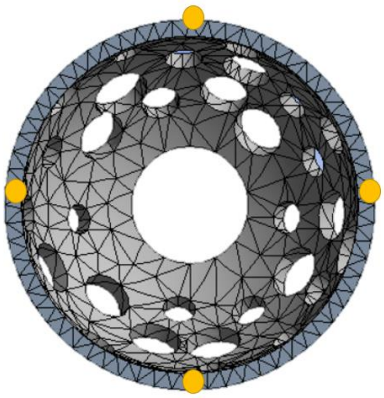

Figure 16- Representation of the adapted reef ball restrained displacement points.

5.7.3. Upwelling reef stability test

For the upwelling reef the results obtained with Ansys® Fluent models were again imported into the Ansys® static structural tool. Next, a mesh was defined for the *upwelling reef* with 7677 nodes and 3459 elements.

Afterwards four displacement points were constrained at the base of the solid, as shown in Figure 17. Then, in each displacement point, a force reaction probe was placed in order to observe the loads evolution at each reaction point.

Finally, four models were computed, one for each inlet velocity.

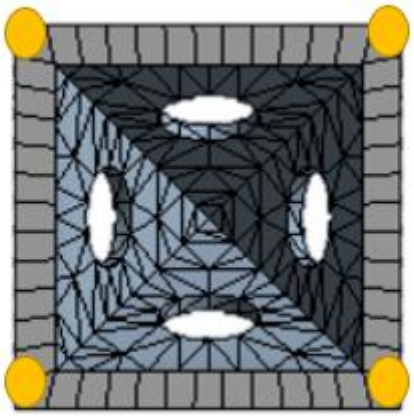

Figure 17- Representation of the upwelling reef restrained displacement points.

5.7.4. Yfalos modular artificial reef stability test

In order to access the stability of the Yfalos modular AR with the configuration that was mentioned above, first the Ansys® Fluent results were imported as pressures to the Ansys® static structural tool. Afterwards a mesh was defined with 6503 nodes and 2862 elements.

Due to the extreme complexity of the configuration that was assembled, and in order to simplify the model, it was assumed only one structure for the analysis, ignoring the fact that niches are made of several units (or pieces). According to this assumption, 4 displacements were restrained at the points represented in Figure 18. In each displacement point, a force reaction probe was placed in order to observe the reaction forces in these points. Four models were computed, one for each inlet velocity.

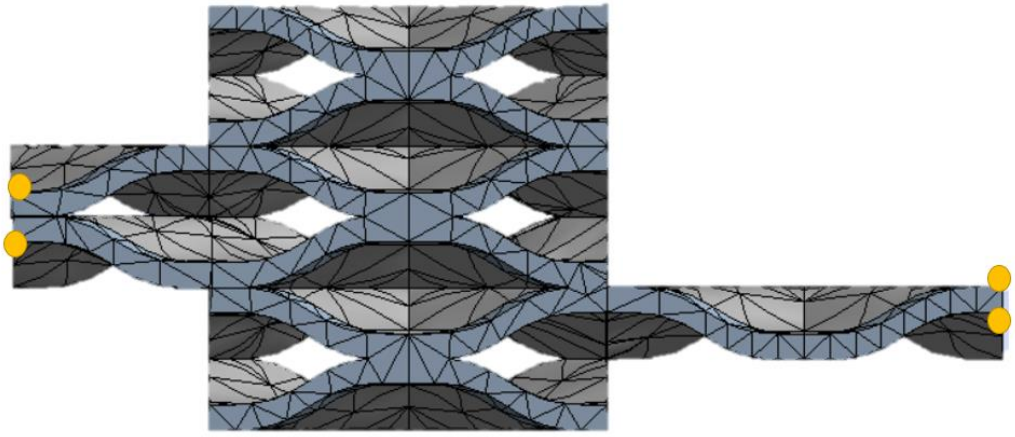

Figure 18- Representation of the restrained displacement points in the Yfalos modular AR

6. Artificial reefs hydrodynamics and design

6.1. Methodology validation

According to the methodology mentioned in the previous chapter, the validation of the procedure used to study the fluid interaction with the AR was based on the results of previous studies (Wang *et al.*, 2018). Considering the geometry of the *cube reef* previously presented, the simulation of the fluid flow was carried out for the same boundary conditions, inlet velocity and fluid properties using Ansys® Fluent (results represented in Figure 19 b)) and REEF3D® (results represented in Figure 19 c)).

After analyzing both results (Figure 19 b) and c)) and comparing them with the results obtained by the authors in the original publication (Figure 19 a)), it is possible to observe that the overall velocity field is essentially similar for all models. The model represented in Figure 19 b) is identical to the original, which is expectable considering that both the simulation parameters and the numerical tool used are the same (Ansys® Fluent). However, it is possible to observe that the original model shows more details of the velocities field, probably because the mesh includes more elements and nodes. Although the number of elements was lower, details and obtained results are quite satisfactory and resemble well the original.

The results obtained with the model that was made with REEF3D® are shown in Figure 18 c). The different aesthetics may be attributed to the fact that it was generated with a different software. The results shown in Figure 19 c) were obtained from the REEF3D® model and visualized using the software package Paraview, which presented a different color pallet when compared to Ansys®. Also, the low flow velocity area forming downstream the cube structure shows to be smaller than in the original model. This may be explained by the timestep that was chosen in the REEF3D® model. Apart from these details, this model also presented satisfactory results.

By comparing the results obtained with the three models, it can be seen that in all cases the highest velocity is reached immediately above the solid (Figure 19 - arrows 1, 3 and 5) while that the fluid flow at downstream and upstream of the solid show lower velocities, (Figure 19 arrows 2, 4 and 6).

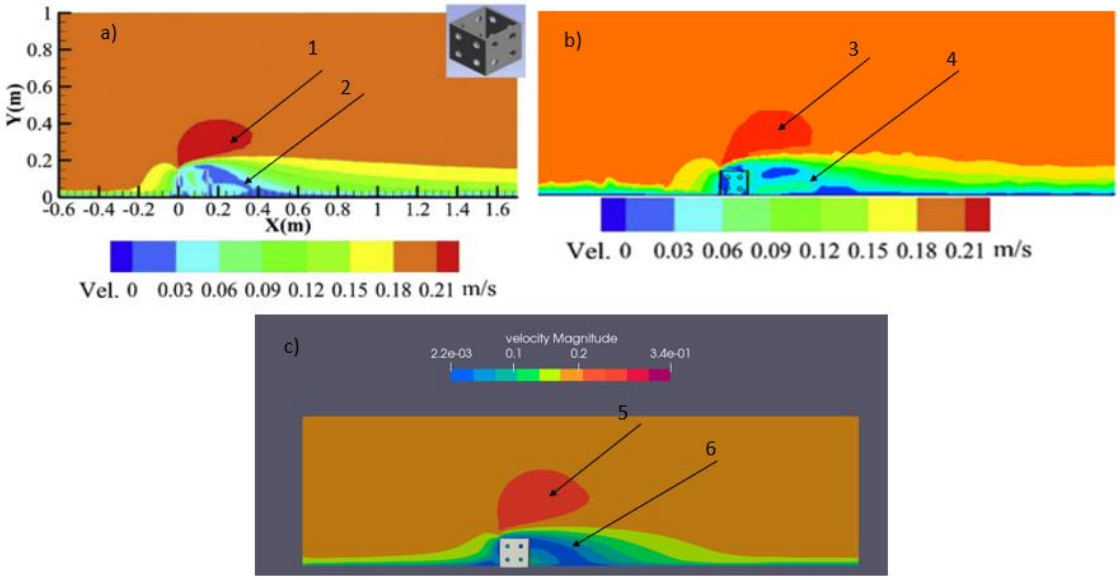

Figure 19- Validations comparison, a) original model adapted from (Wang et al., 2018) ; b) validation with Ansys® Fluent conducted in this dissertation; c) validation with REEF3D®. Arrows indicate high velocity zones (arrows 1, 3 and 5) and low velocity zones (arrows 2,4 and 6).

6.2. Geometry impact on the flow

The AR geometry is absolutely essential to most of the functions that it is intended to perform, including biodiversity promotion, upwelling and erosion control. Therefore, in order to produce AR designs that positively impact the flow and velocity fields, these hydrodynamic interactions need to be carefully analyzed. In this study, the option was to select different AR design concepts in terms of geometry and analyze their impact on the flow, in order to identify particularly interesting features to develop. The simulations conducted are analyzed and discussed in this subsection. Each AR and its interaction with the four inlet velocities are analyzed:1.9 m/s, 0.88 m/s, 0.7m/s and 0.33 m/s.

Only the Ansys® Fluent results will be presented in the following subsections, due to the fact that both software, Ansys® Fluent and REEF3D®, produced similar results, as shown in the Appendix. The results presented in the following chapters adopt a twenty-color pallet (values between 0m/s-2.2m/s). In the Appendix the REEF3D® and Ansys® Fluent results are presented with a velocity scale that changes according to the inlet velocity (v_{in}) regardless of the AR

6.2.1. Cubic artificial reef

The impact produced by the cubic AR on the different flow fields is represented in Figure 20 and Appendix a).

In all the simulations performed (Ansys® and REEF3D®) it was possible to identify a high velocity area in the X, Y plane right above the cubic AR top surface, as represented with arrows 1-4. This area represents the highest flow velocity observable in each simulation reaching values of about 2.2 m/s (v_{in} = 1.9 m/s), 1 m/s (v_{in}= 0.88 m/s), 0.9 m/s (v_{in}= 0.7 m/s) and 0.5 m/s (v_{in}= 0.33 m/s). After observing and carefully analyzing this phenomenon, it is possible to confirm that the higher the values of v_{in}, the higher the velocity in the plume region above the studied AR.

Also, it is visible that in all the models performed (Ansys® and REEF3D®), right after the cubic AR in the downstream direction the velocity of the fluid flow drops to values around 0m/s, where back eddies are generated (arrows 5-12). However, as the distance from the AR increases, the flow in the studied area downstream the solid regains velocity reaching values of 1.8 m/s v_{in} (= 1.9 m/s), 0.6 m/s(v_{in} = 0.88 m/s), 0.5 m/s (v_{in}=0.7 m/s) and 0.2 m/s (v_{in} =0.33 m/s).

At the upstream of the cubic AR the velocity decreases (arrows 13-20) occur, as velocities drop to around 1.3 m/s (v_{in}=1.9 m/s), 0.6 m/s (v_{in}=0.88m/s),0.5 m/s (v_{in}=0.7 m/s) and 0.2 m/s (v_{in} =0.33 m/s).

The flow behavior at the cubic AR sides (right and left according to the X, Y plane) shows two high-velocity “plumes” (arrows 21-28) in both models. Additionally, a closer examination suggests that a higher v_{in} results in higher

velocities at the sides of the solid. This is best observed in the first model (a), which represents a storm scenario [v_{in}= 1.9 m/s]) where velocities of about 2.2 m/s in each side of the structure are observed. On the other hand, the last model (d) corresponds to calm wave scenario [v_{in}= 0.33 m/s]), where the lowest side velocities were reached, with values of about 0.4 m/s. The average and the most frequent wave scenarios (v_{in}=0.88 m/s and v_{in}=0.7 m/s, respectively) result in intermediate velocities.

Inside the Cubic AR, the structure holes promote an increase in the flow velocity (arrows 29-32), that dissipates before reaching the outside of the cube. Velocity increased to around 2.2 m/s (v_{in}= 1.9 m/s),1m/s (v_{in}= 0.88 m/s), 0.9 m/s (v_{in}= 0.7 m/s) and 0.4 m/s (v_{in}=0.33 m/s).

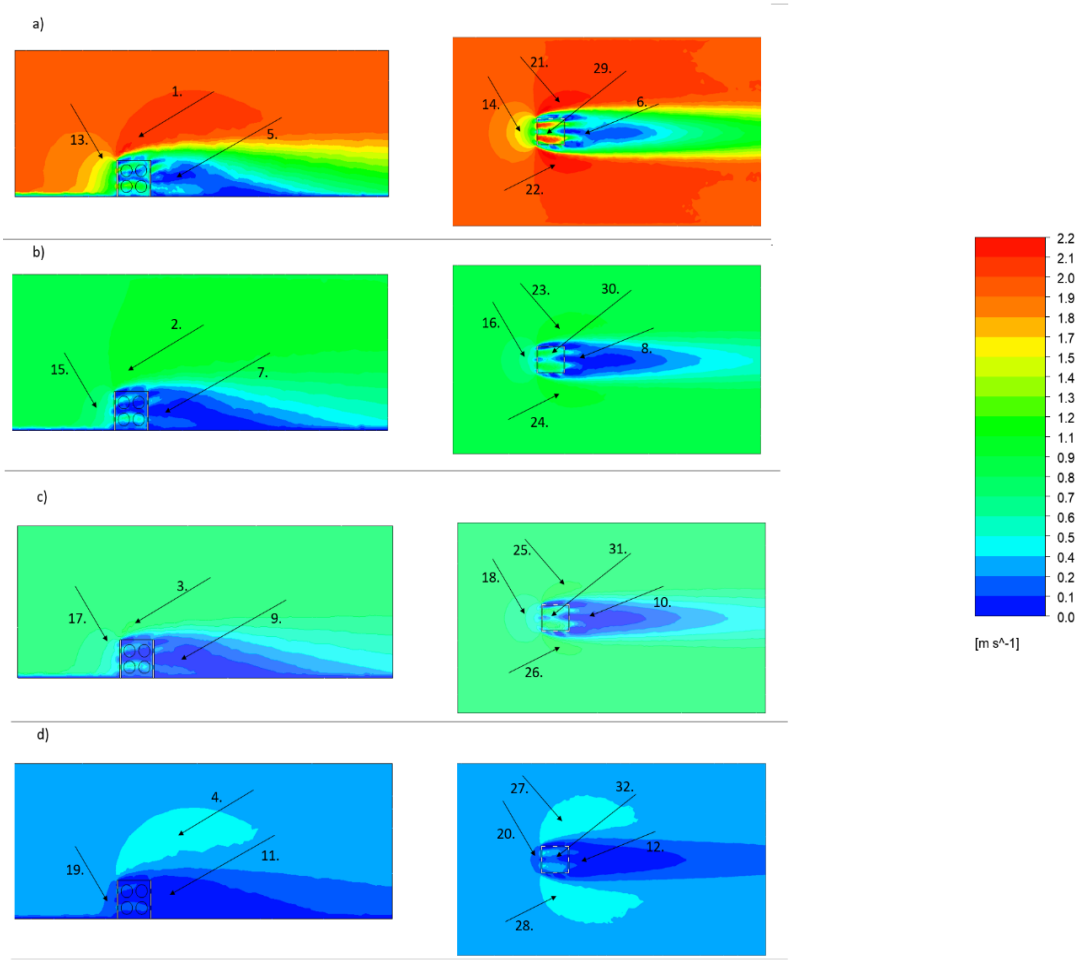

Figure 20-Representation of the cubic AR results where a) represents the results obtained for an inlet velocity of 1.9 m/s, b) represents the results obtained for an inlet velocity of 0.88 m/s, c) represents the results obtained for an inlet velocity of 0.7 m/s and d) represents the results obtained for an inlet velocity of 0.33 m/s

The interaction of a specific flow with a cubic shaped AR was discussed recently by (Galdo *et al.*, 2022). In this study the obtained flow patterns were similar to the results shown in this dissertation, with both REEF3D® and Ansys®. When comparing the geometries (cubic AR adopted in this dissertation and the cubic shaped AR adopted by Galdo *et al.*, (2022)), it is possible to observe that they have in common the overall cubic shape, although minor details like holes and other complexities differ significantly. The reported CFD results presented a plume of high velocity which was referred to as a significant upwelling effect, plus a zone of low velocities found at the downstream of the structure dominated by back eddies (Galdo *et al.*, 2022). Therefore, general similarities in the flow behavior could be identified

Jiang *et al*., 2016 adopted a simple cube with guide plates, with the objective of guiding the flow. In this case the flow patterns obtained were in general similar to the ones previously shown to the cube reef, where the high velocity plume formed above the solid and the zone with the lowest flow velocity located at the back of the AR characterized the main flow results (Jiang *et al.*, 2016). It was also identified by the authors that the inclination of the plates can lead to an increased upwelling effect.

Jiang *et al*., 2010, also tested a cubic shaped AR, and the results obtained show very similar features to the ones previously presented in this dissertation. Once more, the high velocity plume was located above the solid (and again identified as an upwelling effect) while the low velocity zone was forming on the backside of the solid (Jiang *et al.*, 2010). The study that was used for validation purposes, also using a cubic solid showed very similar results regarding the flow field patterns (Wang *et al.*, 2018).

Liu et al, 2012, analyzed the behavior of an open cube, which was subjected not only to a CFD analysis but also characterized in a hydraulic flume using PIV. In this study it was again possible to observe a plume of high velocity above the solid, an area of low velocity that propagates until the end of the domain, and two plumes of high velocity on each side of the structure (Liu *et al.*, 2012), similarly to the results obtained in this dissertation.

The key results of all above-mentioned studies may be summarized by the images presented in Figure 21, where it is possible to see a similar behavior in all the different (cubic) structures. Furthermore, when these are also compared to the results in Figure 2, a similar flow pattern interaction with the cubic structures is observable.

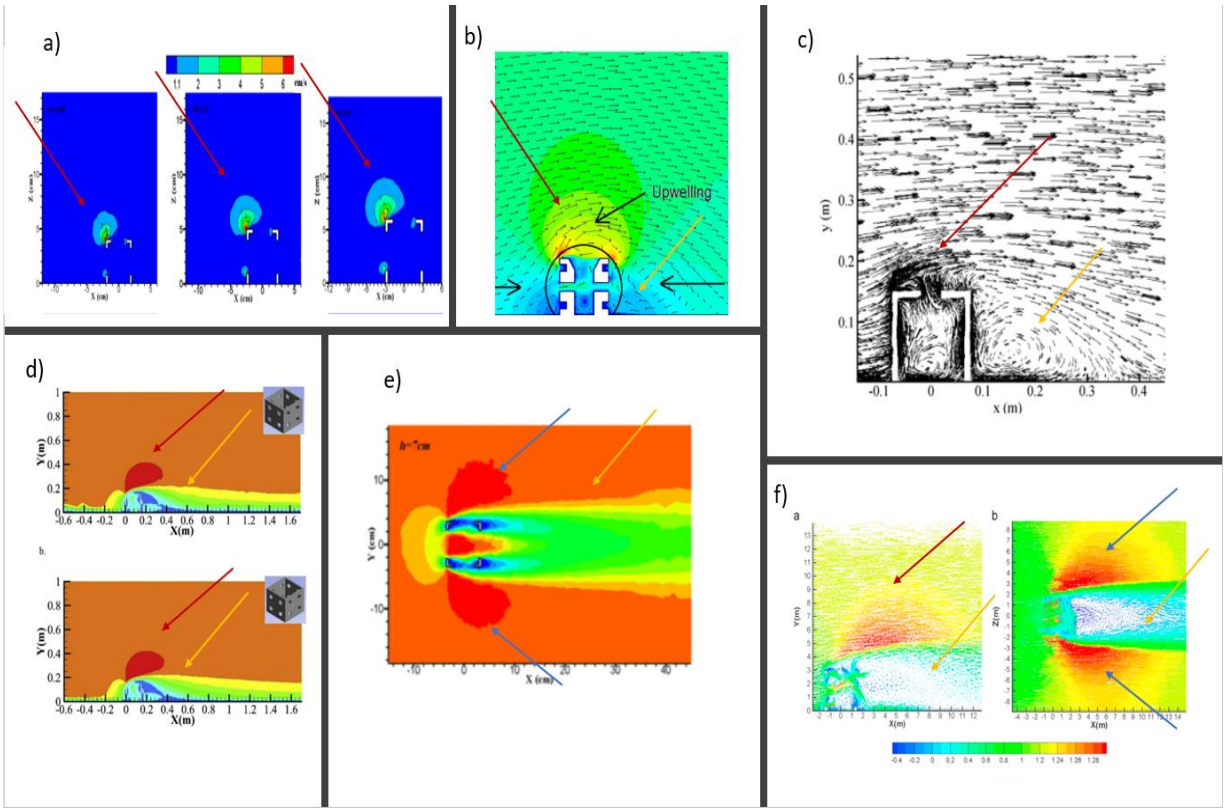

Figure 21-- Previous results in terms of flow velocities around the AR structure, obtained by other authors: a)(Liu et al., 2012); b) (Galdo et al., 2022); c) (Jiang et al., 2010); d (Wang et al., 2018); e) (Liu et al., 2012); f) (Jiang et al., 2016). In this figure the red arrow indicates the location of high velocity plumes present in all the images, the yellow arrow represents the location of low velocities at the back of the cubic structures and the blue arrow represent the location where plumes of high velocity at the sides of the solid are found.

6.2.2. Adapted reef ball

The results obtained for the *adapted reef ball* are shown in Figure 22 and Appendix b). The results were again very similar for both software (Ansys® and REEF3D®).

The adapted reef ball presented different impacts on the fluid dynamics when compared to the cubic AR. The *adapted reef ball* flow simulation results show a

high flow velocity plume on top of the solid (arrow 1-3), as can be seen in the simulations results shown in Figure 22 a), b) and d). The velocities of the top plumes reached values around 2.2 m/s (v_{in}=1.9 m/s),1 m/s (v_{in} =0.88 m/s) and 0.4 m/s (v_{in} =0.33 m/s), respectively. On the other hand, the simulation results shown in Figure 22 c) didn't show the same plume on top of the reef as visible as before, which is very likely related to the scale and color pallet used. Additionally, in general the obtained plumes seem smaller than the ones produced by the cubic AR.

On the structure's backside, and regardless of the v_{in}, the fluid velocity drops to values of about 0m/s and back eddies are generated (arrows 4-11). Then, and with increasing reef distance, a velocity increase was observable in the order of 1.8 m/s (v_{in} =1.9), 0.7 m/s (v_{in} =0.88m/s), 0.6 m/s (v_{in} =0.7 m/s) and in the last case the velocity reached the same values of the v_{in} (v_{in} =0.33 m/s).

Also, on the front side of the *adapted reef ball* structure, a low-velocity zone was observable (arrows 12-19), with values in the order of 1.3 m/s (v_{in} =1.9 m/s), 0.6 m/s (v_{in} =0.88 m/s), 0.5 m/s (v_{in} =0.7 m/s) and 0.2 m/s (v_{in} =0.33 m/s).

On the other hand, the sides of the adapted reef ball formed plumes of high velocities (arrow 20-27), the velocities of this plumes are in the order of 2.2 m/s (v_{in} =1.9m/s), 1 m/s (v_{in} =0.88 m/s), 0.9 m/s (v_{in} =0.7 m/s) and 0.4 m/s (0v_{in} =.33 m/s). These plumes seem much smaller in size than the ones generated by the cubic AR.

Inside the *adapted reef ball*, relatively low velocities were detected, with values in the order of 0.8 m/s (v_{in} =1.9 m/s), 0.2 m/s (v_{in} =0.88 m/s and v_{in} =0.7m/s) and 0.1 (v_{in} =0.33 m/s). The solid's holes don't seem to accelerate the flow as much as previously found for the cubic AR, which could be due to their small size.

When the results of the *adapted reef ball* are compared with the cubic AR, it is clear that the cubic AR has a greater impact on the flow field than the adapted reef ball. Also, when comparing the results shown in Figure 22 with the appendix b) (Ansys® and REEF3D®) it is possible to observe some differences that are directly related to the different velocity scales (color pallet) that were used.

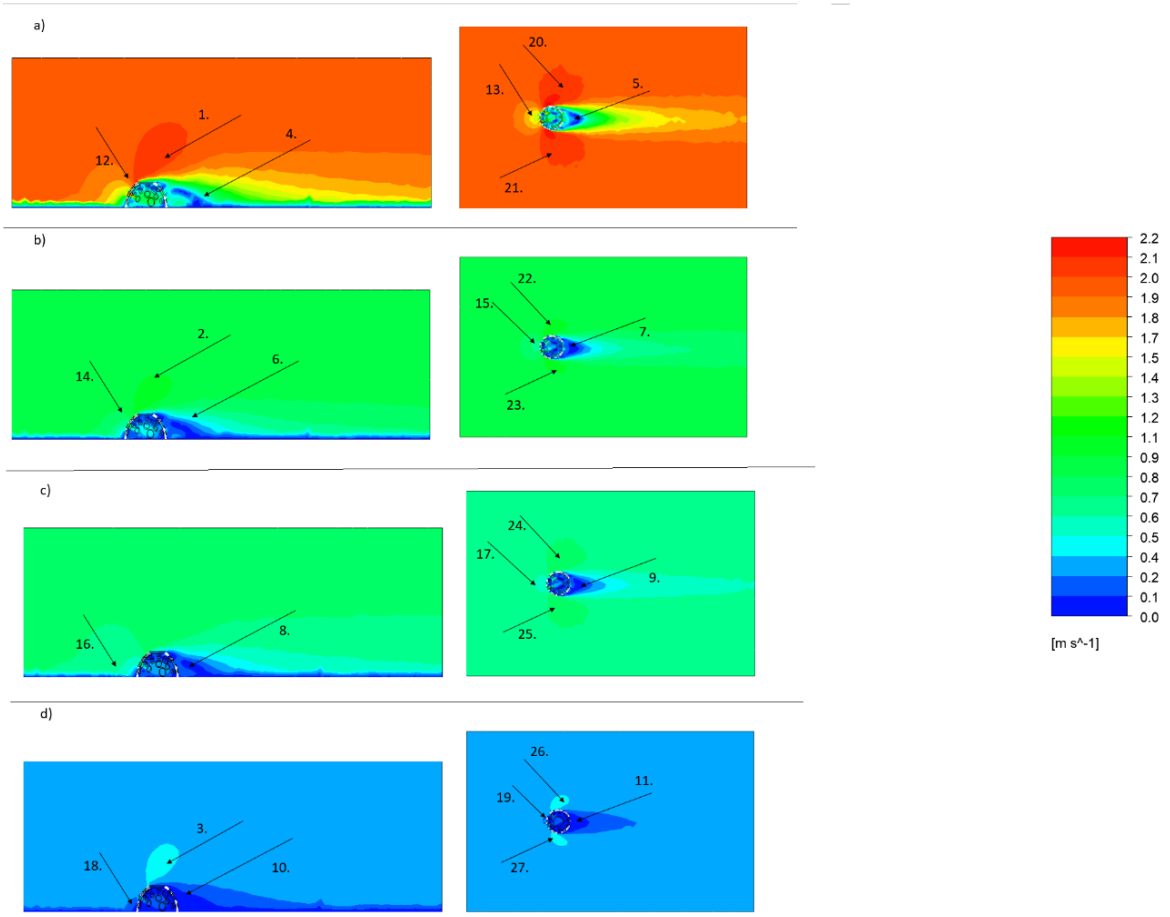

Figure 22- Representation of the adapted reef ball results where a) represents the results obtained for an inlet velocity of 1.9 m/s, b) represent the results obtained for an inlet velocity of 0.88 m/s, c) represent the results obtained for an inlet velocity of 0.7 m/s and d) represent the results obtained for an inlet velocity of 0.33 m/s.

After comparing the results obtained for the *adapted reef ball* with other studies that used spherical geometries with potential for application in ARs, similarities in the flow patterns were found. A semi-spherical AR in the shape of a “bicycle helmet” was analyzed by (Ahmed *et al.*, 2016). This AR was studied in a CFD simulation using Ansys®, where a high-velocity plume on the top of the spheric AR was reported. The high-velocity plume above the solid, that was produced by the “bicycle helmet” shaped AR, had different dimensions from the *adapted reef ball*, which could be partially related to the size or scale, or the different geometry.

A semi spherical AR was also adopted by (Luiyi *et al.*, 2017) to observe and compare the fluid behavior. A high-velocity plume was reported on top of the AR,

plus two high-velocity plumes at the sides (right and left) of the structure. When comparing these findings to the results observed in the current dissertation, it is possible to identify similar characteristics in the fluid propagation. Although, the results are somewhat similar, some differences may be identified, which could be explained by the different scales and/or the absence of a top cover.

(Le, Jung and Na, 2020) analyzed different ARs using numerical simulations, whereas one of them was a reef ball. It was reported that the reef ball produced a “wake region”, referring to the flow movement towards the inlet’s direction. In our findings no model presented a flow moving backwards as described in the article, which might be caused by the different geometry or specific current conditions.

Figure 23 represents a summary of the main findings of the review conducted on the above-mentioned articles. The flow patterns induced by the *adapted reef ball* has some similarities to the ones presented in Figure 23 (a) and (b) considering that both generate a plume of high velocity above the solid (blue arrow). In the case of Figure 23 b) it is also possible to observe the high velocity plumes on the sides of the solid (black arrows). Additionally, in Figure 23 a) it is also possible to observe a similar fluid behavior on the back of the solid (green arrow) dominated by low velocities. The results shown in Figure 23 c) are somewhat different from the patterns obtained with the adapted reef ball in this dissertation, probably due to a flatter geometry.

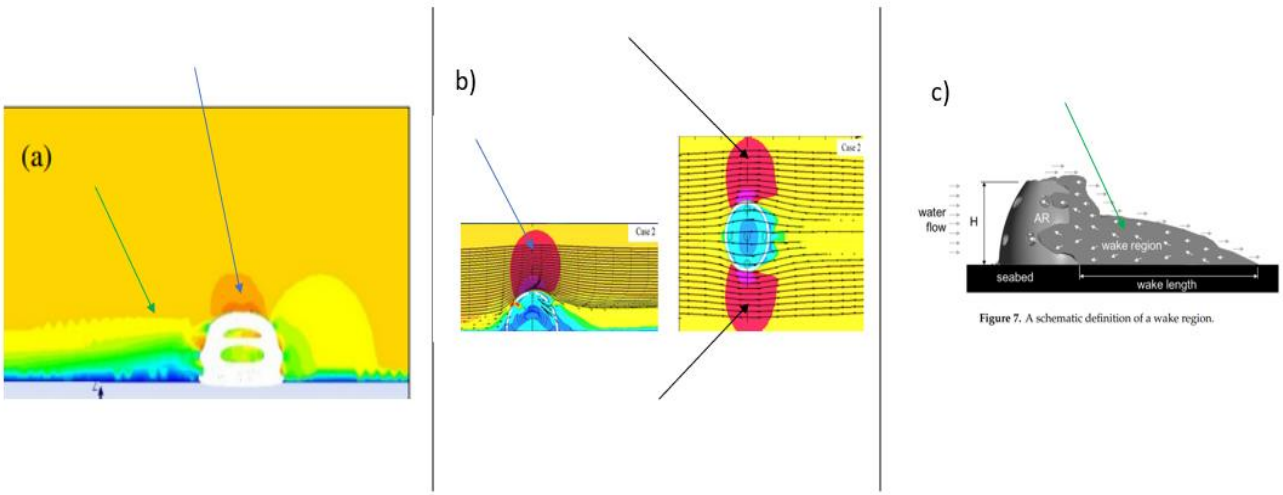

Figure 23- Representation of previous results using spherical ARs. a(Ahmed et al., 2016); b) (Luiyi et al., 2017); c) (Le, Jung and Na, 2020). The blue arrow indicates the location of the high velocity plume above the solid, the black arrow indicates the high velocity plumes, and the green arrows indicate the flow-behavior at the back of the solid.

6.2.3. Upwelling reef

The results obtained for the *upwelling reef's* effect on the flow hydrodynamics are presented in Figure 24 and Appendix c). In the simulations conducted large high velocity plumes on top and sides of the *upwelling reef* were obtained, apparently larger than the ones obtained in any of the previous analysis. Also, it is possible to observe that the area in the back of the solid also impacts significantly the flow and pronounced back eddies are generated in this region.

Both REEF3D® and Ansys® simulations regarding the *upwelling reef* resulted in the identification of high-velocity plumes above the structure (arrows 1-4) and on the sides (right and left) (arrows 21-28), which present maximum velocity values in the order of 2.2 m/s (v_{in} =1.9 m/s), 1m/s (v_{in} =0.88), 0.9 m/s (v_{in} =0.7 m/s) and 0.4 m/s (v_{in} =0.33 m/s).

Similarly, to the other reefs, the flow velocity decreases to almost 0 m/s at the immediate backside of the reef with the generation of back eddies, which are visible both in Ansys® and REEF3D® analysis. Again, when increasing the distance from the solid in the downstream direction, the flow velocity seems to increase, although never reaching the same velocity as the inlet, while maximum velocities of 1.7 m/s (v_{in} =1.9m/s), 0.8 m/s (v_{in} =0.88 m/s), 0.7m/s (v_{in} =0.7 m/s) and 0.3 m/s (v_{in} =0.33 m/s) were reached.

On the solid's front side, low-velocity areas are generated (arrows 13-20) with velocities of around 1.3 m/s (v_{in} =1.9 m/s), 0.6 m/s (v_{in} =0.88), 0.5 m/s (v_{in} =0.7) and 0.2 (inlv_{in} = 0.33), possible to observe in the results from both software. Additionally, it is possible to observe a high velocity area generated in the direction of the *upwelling reef* main hole, which is visible in all the simulations presented in Figure 24.

Overall, when comparing the results of the *upwelling reef* to the previous two reef geometries, results show that the flow patterns are somewhat similar to those produced by the cubic AR. However, the impacted area is clearly larger in the *upwelling reef* case. Regarding the flow patterns on the sides, top and back of the solid, it is possible to identify the high velocity plumes formed on the top and sides, and a low velocity area in the downstream with significantly larger dimensions in the back of the solid.

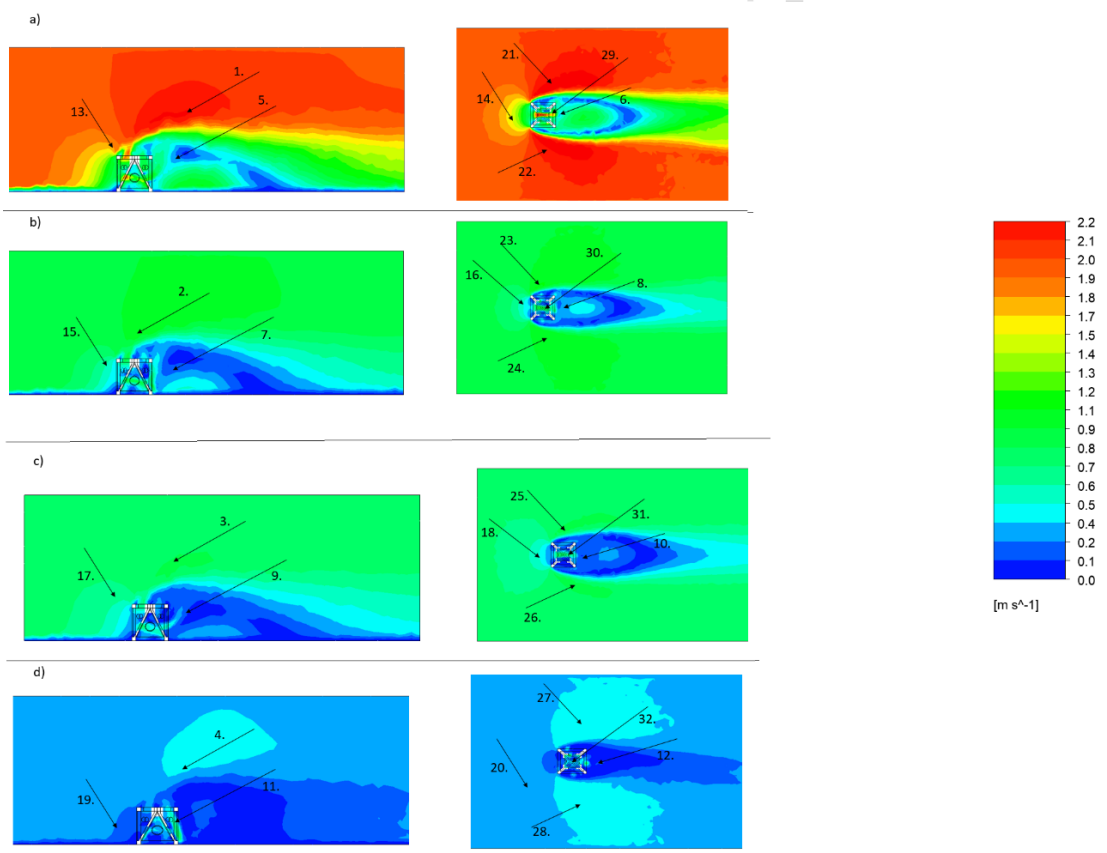

Figure 24-Representation of the upwelling reef interaction with the fluid; a) results for an inlet of 1.9 m/s; b) for an inlet of 0.88 m/s; c) for an inlet of 0.7 m/s and d) for an inlet of 0.33 m/s.

The upwelling reef is a cube with four isosceles triangles inside. Therefore, it is possible to observe similar fluid patterns to the ones obtained with cubic AR, although the size of the affected area was much larger when the *upwelling reef* was studied. These differences may be attributed to the “pyramid” shape inside the cube, as suggested by another study from (Jiang, Liang and Tang, 2019) where the upwelling reef was reported to have “a wider range, higher upwelling height, and more complex flow patterns” (Zhang *et al.*, 2021). When comparing the results that were obtained in the current dissertation with the reported results in (Jiang, Liang and Tang, 2019) using the same solid, very similar flow patterns are observable, as shown in Figure 25.

Furthermore, when comparing the upwelling reef results with past reports related to the flow patterns in *cubic reef* models (Figure 21), a certain similarity in the flow patterns is observed, especially regarding the high-velocity plumes on the top and sides, and the back eddies region.

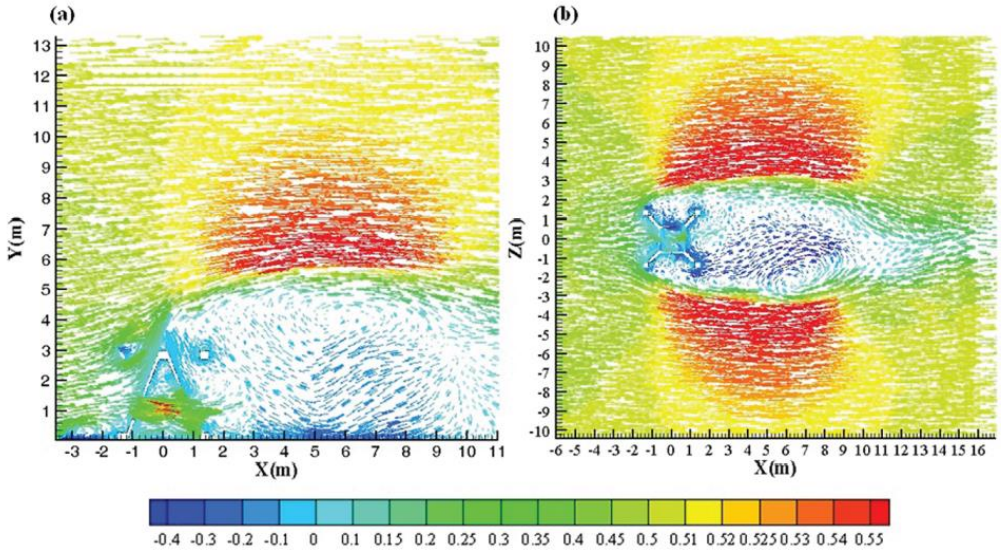

Figure 25- Representation of velocity (m/s) flow results using the upwelling reef (Jiang, Liang and Tang, 2019).

6.2.4. Yfalos modular artificial reef

The results obtained for the Yfalos modular AR are represented in Figure 26 and Appendix d). Again, the results of both software (Ansys® and REEF3D®)

were very similar. This structure produced the smallest areas regarding high flow velocity plumes above the solid (arrow 1-2) comparing to the previous ARs, with velocities about 2.2 m/s (v_{in} =1.9 m/s) and 0.4 m/s (v_{in} =0.33 m/s)

In this case the AR only presented high velocity plume above the solid in the simulation a) and d) (v_{in} =1.9 m/s and v_{in} = 0.33 m/s respectively) of the simulations, which might be due to the color pallet that was used in the results presentation (if a different color ranges were implemented in current the model it might be observable local upwelling in all the simulations.

In the front side of the solid a low-velocity zone is formed (arrows 1-8) showing values of about 1.3 m/s (v_{in} =1.9 m/s), 0.6 m/s (v_{in} =0.88), 0.5 m/s (v_{in} =0.7) and 0.2 (v_{in} =0.33).

At the downstream direction of the solid the velocity was also low and dominated by back eddies (arrows 9-16), whereas the further away from the solid the more the velocity seems to increase, with maximum observable velocities of 1.8 m/s (v_{in} =1.9m/s), 0.8 m/s (v_{in} =0.88 m/s), 0.6m/s (v_{in} =0.7 m/s), and in the last simulation reaching the same velocity as the v_{in} (v_{in} =0.33 m/s).

Also, two high-velocity plumes are observed on the sides of the solid (arrows 19-24), the values were around 2.2 m/s (v_{in} =1.9 m/s),1m/s (v_{in} =0.88 m/s), 0.9 m/s (v_{in} =0.7 m/s) and 0.4 m/s (v_{in} =0.33 m/s).

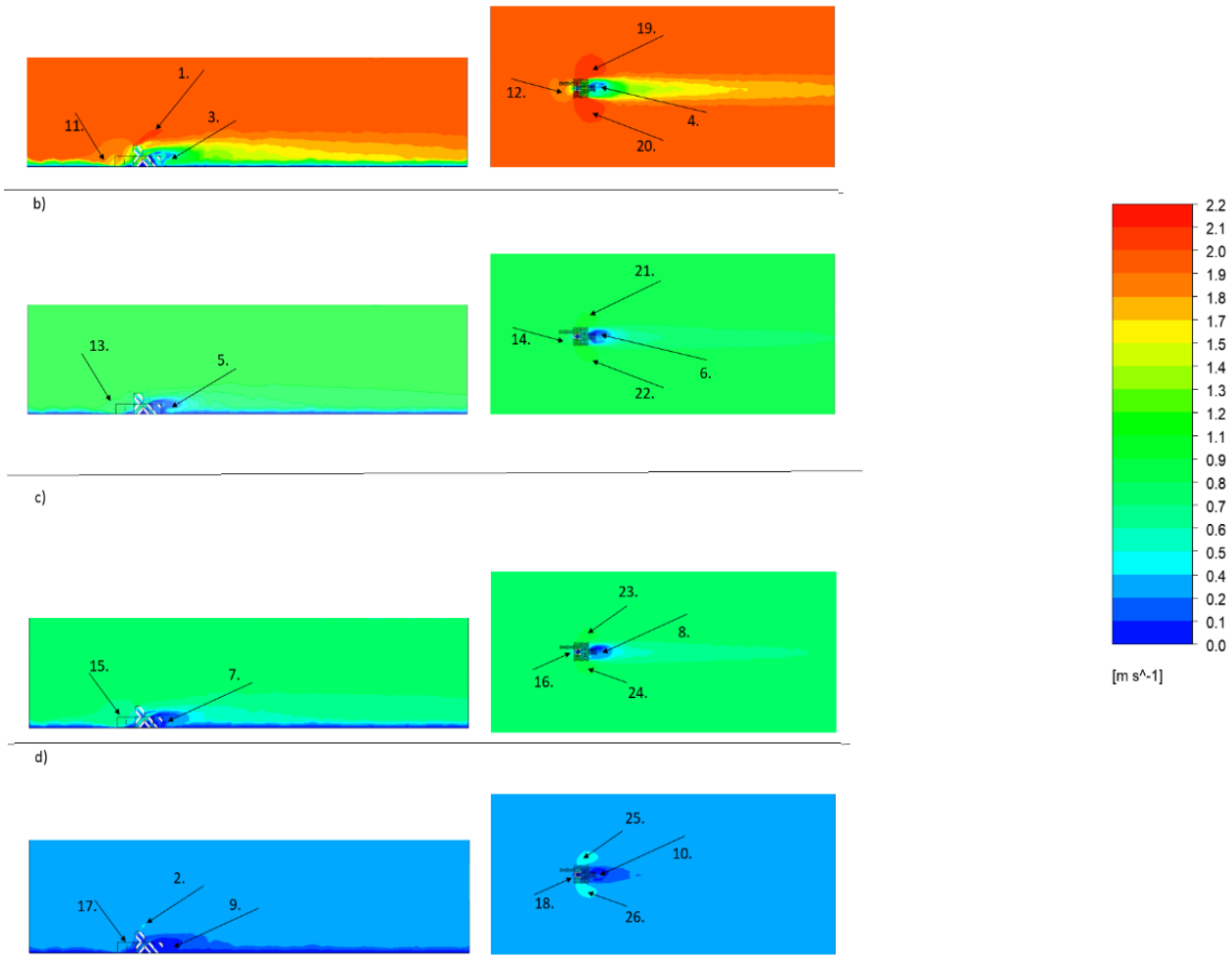

Figure 26- Representation of the Yfalos modular AR results where a) represents the results for an inlet velocity of 1.9 m/s, b) represents the results for an inlet velocity of 0.88 m/s, c) represents the results for an inlet velocity of 0.7 m/s and d) represents the results for an inlet velocity of 0.33 m/s.

When comparing the results presented in Figure 26 with the appendix d) it is possible to observe some differences especially regarding the case d) where the area in reef downstream reaches the same flow velocity as the inlet velocity, while in the Appendix d) there is an extension of low velocities that spreads beyond the end of the domain.

When comparing the Yfalos modular AR, with this specific configuration, with the previously mentioned reefs, the overall impact on fluid flow seems less significant, as all of the formed plumes which seem smaller than the ones from the previously analyzed reefs, and no plume was formed on top of the solid.

Due to being made out of modules, this type of AR has several advantages such as being easy to work with, in terms of size and configuration, since it is only

necessary to alter the size of one module and the configuration size also changes. This feature also allows a vast variety of configurations, with a variety of modules, which can be adapted and altered according to different purposes and needs (Designboom, 2021).

6.2.5. Ansys® Fluent vs REEF3D®

Both Ansys® Fluent and REEF3D®, presented interesting results, even though they were applied with models of different scales and similar fluid characteristics. Nevertheless, some differences were observed between the results obtained with the two software, such as in the case of the *adapted reef ball*, for which the high velocity plumes in the side or top of the solid, were not visible in the REEF3D® results. This type of inconsistencies could be justified by several factors:

As it was mentioned before in the methods section, in both cases the same viscosity and water density were adopted. Those values might need to be changed, in order to consider the geometrical scaling of 1:20. When assumed in the methods that both real size and scaled models have the same water parameters, that implies that both models also have different Reynolds coefficients (Silva, 2019). In fact, the scaled models have a Reynolds coefficient 20 times smaller than the real scale models, which explains the small differences between the results obtained with the Ansys® Fluent and REEF3D® models. In order to maintain the Reynolds coefficient unchanged in the REEF3D® model, for example the viscosity of the fluid would have to be adapted.

Also, as mentioned before both software used different equations to solve the flow variables. In Ansys® the k-ε RNG equation was used, while in REEF3D® the standard k-ε equation was employed. This factor might also lead to some differences between models.

Another factor that might have been responsible for small is the time-step that was used on the REEF3D® analysis, which can also influence the final result.

Overall, in both cases the simulations returned consistent numerical results with similarities.

6.3. Uplift/upwelling and eddies effects

As mentioned before, the upwelling effect has an huge impact on the trophic cascade, laying out the conditions for phytoplankton to grow and, afterwards, allowing it to be consumed by larger predators (Largier, 2020). In previous studies it was claimed that ARs can generate local upwelling (or uplift) (Galdo *et al.*, 2022), whereas the criteria for the identification of local upwelling, induced by structures, was as follows: “when the region above the structure exceeds 1.05 times the incoming velocity that region is defined as an upwelling region” (Jiang *et al.*, 2013, 2016; Wang *et al.*, 2018).

The results that were obtained in section 6.2 demonstrated that the high velocity plume which was generated above some of the ARs exceeded 1.05 times the incoming velocity, which means that these high velocity plumes can be defined as upwelling regions (Jiang *et al.*, 2013, 2016; Wang *et al.*, 2018) or local upwelling. Taking these facts into consideration, it is possible to assume that the structures that were analyzed in this study are able to generate a local upwelling region.

Assuming the previous premises it is possible to observe that *the upwelling reef* might produce a larger and stronger local upwelling (or uplift) region than the remaining structures, which might enhance the local biological production, including fish biomass (Leitão, 2013). It is also observable that, according to the results the *Yfalos modular AR* with the configuration that was used, it might produce a less effective local upwelling than the remaining structures. The *cubic AR* and the adapted reef ball may produce an upwelling with an efficiency between the two remaining structures (lower than the *upwelling reef* and higher than the *Yfalos modular AR*).

Furthermore, previous research also mentioned that the AR downstream, where eddy currents are generate with stable low flow velocity, provides favorable conditions for the fish to group (Wang *et al.*, 2018). In the results (section 6.3) it

is shown that the upwelling reef also seems to produce the wider low velocity area dominated by back eddies, which might suggest that the upwelling reef would also produce a larger area for the fish to group, according to previous assumptions (Wang *et al.*, 2018).

6.4. Holes and cavities

According to previous research, the holes on a structure represent the most important characteristic for the colonization of the AR (Hixon and Beets, 1989; Jiang *et al.*, 2020). It is also claimed that a reef with more holes should support more fish (Hixon and Beets, 1989).

Assuming these premises, the *adapted reef ball* and the *cubic AR* possess more holes than any of the other solids, which might be the most attractive AR in terms of colonization. The upwelling reef design count with 12 holes, thus allowing fish and cephalopods to pass (Jiang, Liang and Tang, 2019), as well as may also be an attractive structure to colonize.

The Yfalos modular AR doesn't present holes, although it presents itself as a semi-open structure, with the objective of "creating habitat for different marine species and by preventing illegal fishing (like troweling)" (Designboom, 2021).

6.5. Structural stability

According to previous studies the stability is a major concern when deploying an AR (Liu et al., 2007), due to the potential of overturning as a result of strong and unbalanced currents.

When analyzing the stability results regarding the *cubic AR* represented in Figure 27, one can observable that a higher inlet velocity leads to a more unstable structure.

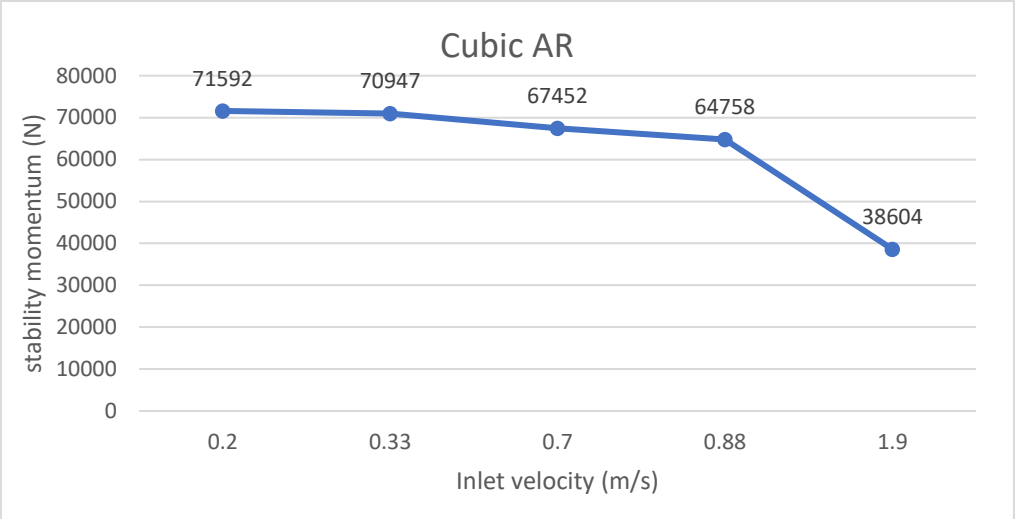

Figure 27- Stability results for cubic AR.

The stability results regarding the adapted reef ball represented in Figure 28 indicate a different tendency when compared to the cubic AR. Here, a higher inlet velocity leads to a more stable structure, although, the loads present lower values on the *adapted reef ball.*

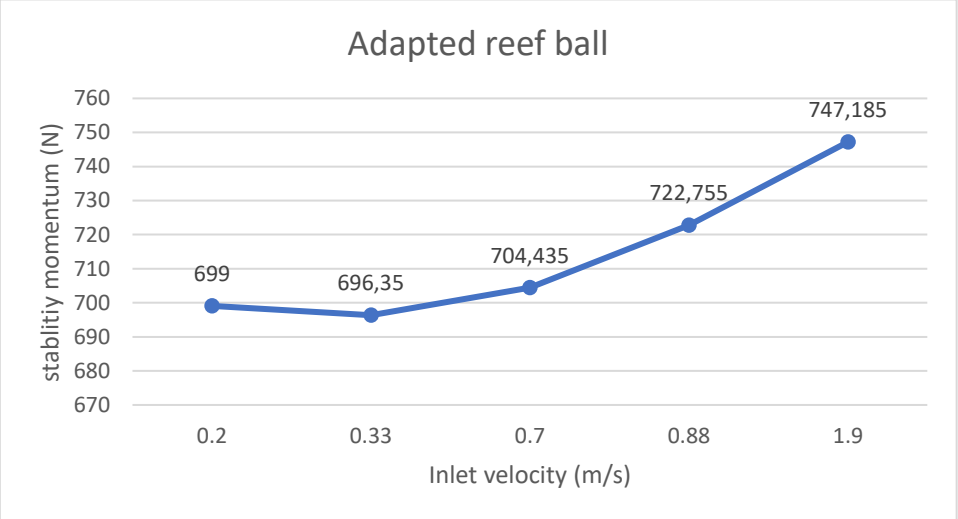

Figure 28- Stability results for adapted reef ball.

The *upwelling reef* stability results presented in Figure 29, show that the upwelling reef is the most stable among all ARs studied. Also, it is possible to observe that a higher inlet velocity leads to higher stability, which is in accordance with what the authors claim. Authors explain that *upwelling reef* is prepared to deal with an absence of a bottom cover in order to produce a “vac-sorb, which prevents the

reef from trapping, moving, or falling, even on a muddy sea floor" (Jiang, Liang and Tang, 2019).

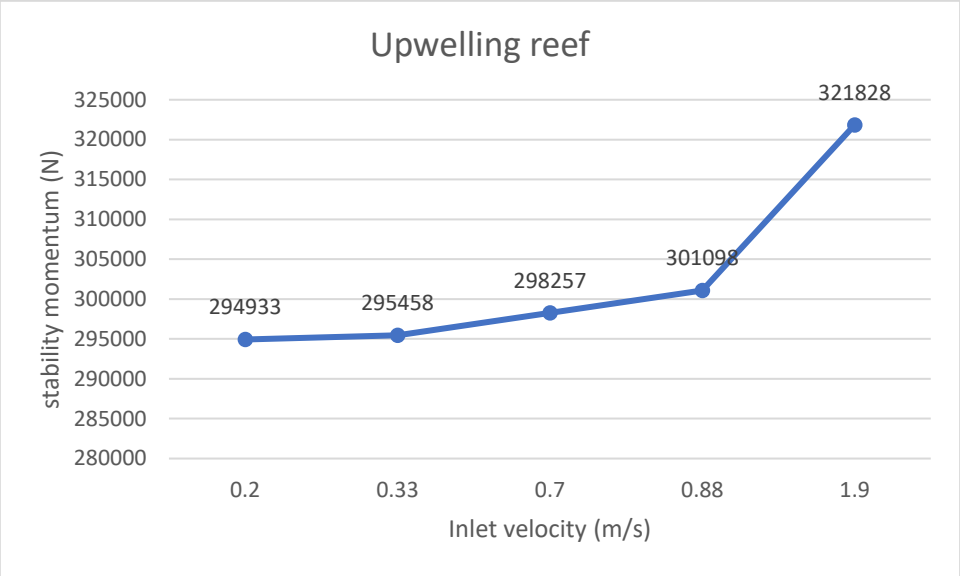

Figure 29- Stability results for upwelling reef.

The Yfalos modular AR results are presented in Figure 30 and show that when assuming the configuration as only one piece, a higher velocity leads to a lower structural stability. The Yfalos modular AR presented a higher stability than the adapted reef ball and a lower stability than the remaining ARs, although these results consider that all pieces composing the Yfalos niche are able to maintain their integrity and remain assembled as one.

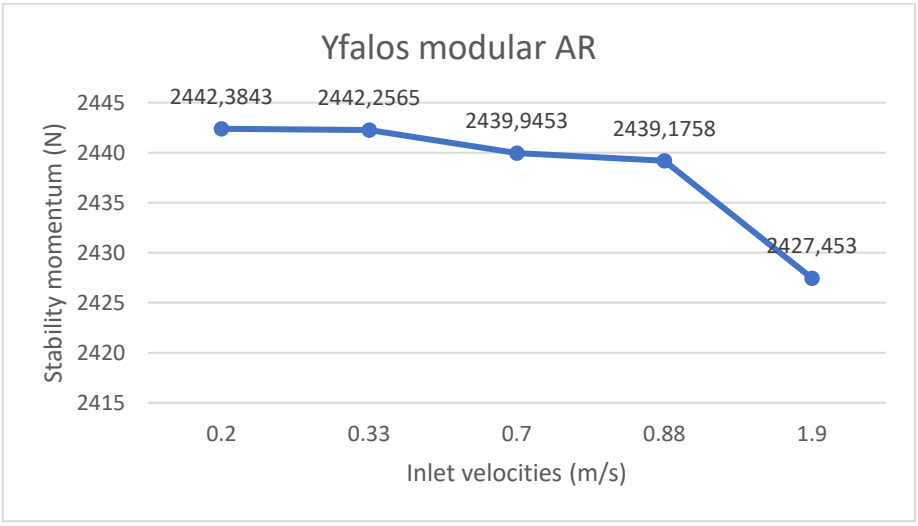

Figure 30- Stability results for the Yfalos modular AR (with the configuration mentioned previously).

6.6. Erosion

One of the main issues associated to the deployment of ARs in coastal environments is the local scouring near the reef. Scour is described as localized removal of sediment around an object by waves and currents (Raineault *et al.*, 2013). Whenever scour occurs changes might be observed in sediment grain size distribution (Raineault *et al.*, 2013) and the foundation may become unstable (Dwito Armono and Wirayuhanto, 2018). When the foundation becomes unstable the AR structure may eventually overturn and lose its stability (Dwito Armono and Wirayuhanto, 2018). In previous investigation this phenomena was observed while affecting structures in different ways such as eroding the area around and inside of an AR (Tang *et al.*, 2021), and creating scour holes on the structure sides (Düzbastilar *et al.*, 2006).

Scouring near the ARs, according to past researches, might be linked with the high velocities produced by the interactions of the fluid and the solid (Jiamei *et al.*, 2020; Santoro *et al.*, 2022).

Assuming the premises mentioned before, the *upwelling reef* might present the highest rates of scouring while the *adapted reef ball* and the *Yfalos modular AR* might present the lowest scouring due to the lower values of the maximum velocities they generate. Also, the *cubic AR* and the *adapted reef ball* may produce scour with rates between the two remaining structures (smaller than the *upwelling reef* and higher than the *Yfalos modular AR*).

Also, as mentioned by multiple authors(Van Rijn, 1993; Yun and Kim, 2019), methods may be applied to mitigate the scouring issue, such as the use of a geogrid (a foundation placed underneath the solid) (Yun and Kim, 2019) which decreases the maximum velocities, as well as placing coarser sediments near to the AR (Van Rijn, 1993).

Based on the results obtained, the critical velocities for erosion could have been calculated and compared to the velocities obtained near the reef structures studied. However, it was not possible to complete the sizing analysis of a typical sediment from the possible case study location. With this information, possible

erosion areas arround the structures studied could have been estimated. This challenge is left for future developments.

6.7. Section conclusions

After reviewing the results, it is possible to conclude that different reef geometries influence the flow field differently. Also, for the chosen conditions the *upwelling reef* can be highlighted for having a greater impact on the fluid behavior. In contrast, the *Yfalos modular AR* showed the smallest impact on the flow field. It was also possible to observe that the *cubic AR* and the *upwelling reef* results were relatively similar in terms of flow patterns, although the impacts were amplified whenever the *upwelling reef* was used. The adapted reef ball presented a relatively small impact in the flow field, when compared to the *cubic AR* and *upwelling reef*.

Concerning the stability, the *upwelling reef* presented a higher stability than the remaining structures, the *adapted reef ball* seems to be the less stable structure and the *Yfalos modular AR* and the *cubic artificial* presented intermedium values.

It was also concluded that both REEF3D® and Ansys® fluent are efficient alternatives to support the design of Artificial Reefs regarding their hydrodynamic behavior and interaction with the surroundings in coastal environments.

7.Conclusion and future work

ARs are seen as part of promising strategies to promote coastal and ecosystems restoration. However, the processes to follow in order to achieve efficient and tailored designs are still unclear and in need of further research. This dissertation was aimed at analyzing the impact of different geometries on the local environment, considering the hydrodynamic behavior analysis of different AR proposals found in the literature. These structures were subjected to the action of currents obtained after the analysis of coastal data.

All the ARs that were examined in the current dissertation show an interesting potential to rehabilitate the coastal environment, although due to conditions and objectives that were defined, some ARs might have a better performance than other for the analyzed parameters.

In terms of biological enhancing potential and/or creating a recreational area, the *upwelling reef* seems to show the best arguments for the chosen conditions. The *upwelling reef* seems to produce the strongest upwelling effect, which is a determinant factor on the primary production growth. At its backside, a low velocity area dominated by back eddies is generated, which would be an area that might attract local fish. Furthermore, the holes in the upwelling reef also might play an important role on the habitat potential, according to previous research. Furthermore, the upwelling reef seems to be the most stable of all the analyzed geometries.

Even though the *Yfalos modular AR* didn't present a significant upwelling effect in comparison with the other solids, it still might be a good alternative for shallower waters, taking into account the easy assembling of the configurations and also the fact that, at another velocity scale, it might allow the visualization of local upwelling and back eddies. Overall, the *Yfalos modular AR* seems an interesting approach considering the innumerous possible configurations that it allow, affecting in innumerous different ways the flow field.

The *adapted reef ball* results displayed a small impact on the flow field when compared to the other solids such as the *upwelling reef*, although it might be a

viable option in certain environments since it has an adequate quantity of holes, which according to past studies is considered as a key characteristic for habitat creation.

The *cubic AR* could also be a good alternative for biological enhancement since it might produce a strong local upwelling and back eddies which represent key characteristics for prospective habitat creation. Additionally, it counts with a reasonable number of holes, which according to bibliography, might attract fish.

In the current dissertation the scouring was not fully analyzed. It is an important factor that should be explored before any deployment, which could change the stability results that were performed. Even though, according to the performed literature review where several hypotheses were considered, the chances of scouring are highest with the *upwelling reef* due to the large areas where the high velocity plumes on the sides are formed.

The results, discussion and conclusion demonstrate that the upwelling reef might be the best design for the condition of the study area

The methodologies REEF3D® and Ansys® demonstrate a huge potential in terms of modeling and planning. The REEF3D® was tested in the current dissertation so that in the future, wave, current and sediment transport models could be developed.

In the future, only the REEF3D® methodology will be used to generate a model which includes the effect of waves, currents and sediment transport, in order to understand how each geometry might affect a control environment. Additionally, the effect of considering the placement of reef niches, composed of nearly placed multiple pieces, and their interaction, will be analyzed. Afterwards a high-quality topography will be used on REEF3D® to understand how target geometries might behave under “real conditions”. These models are planned to be developed in a supercomputer.

8.Bibliographic references

Ahmed, Y. M. *et al.* (2016) 'Studying the Hydrodynamic Characteristics of New Type of Artificial Reef', *Journal of Advanced Research Design*.

Alves, B. *et al.* (2015) 'Coastal erosion perception and willingness to pay for beach management (Cadiz, Spain)', *Journal of Coastal Conservation*. doi: 10.1007/s11852-015-0388-6.

ANSYS.inc (2013) *ANSYS Fluent Theory Guide*. Available at: http://www.pmt.usp.br/academic/martoran/notasmodelosgrad/ANSYS Fluent Theory Guide 15.pdf.

Ansys (2021) *Ansys Fluent*. Available at: https://www.ansys.com/products/fluids/ansys-fluent.

Arnouil, D. S. (2008) *Shoreline Response for a Reef Ball Submerged Breakwater System Offshore of Grand Cayman Island*. Florida Institute of Technology in partial fulfillment of the requirements for the degree of Master of Science in Ocean Engineering.

Autodesck (2022) *Autodesck CFD*. Available at: https://www.autodesk.com/products/cfd/overview.

Awang, D. and Pit, I. B. (2003) 'Study On Reef ball At Batu Penyu nearby Talang Talang Island', *Institut Penyelidikan Perikanan Malaysia Sarawak (Fisheries Research Institute)*.

Barber, T. R. and Barber, G. L. (1996) 'REEF BALL'.

Bihs, H. (2021) *REEF3D:: User Guide*. Associate Professor Marine Civil Engineering NTNU Trondheim.

Black, K. P. *et al.* (2020) 'Salient Evolution and Coastal Protection Effectiveness of Two Large Artificial Reefs', *Journal of Coastal Research*. doi: 10.2112/JCOASTRES-D-19-00117.1.

Boström, C. and Mattila, J. (1999) 'The relative importance of food and shelter for seagrass-associated invertebrates: A latitudinal comparison of habitat choice by isopod grazers', *Oecologia*. doi: 10.1007/s004420050845.

Botsford, L. W. *et al.* (2006) 'Effects of variable winds on biological productivity on continental shelves in coastal upwelling systems', *Deep-Sea Research Part II: Topical Studies in Oceanography*. doi: 10.1016/j.dsr2.2006.07.011.

Carvalho, A. N. and Santos, P. T. (2013) 'Factors affecting the distribution of epibenthic biodiversity in the Cávado estuary (NW Portugal)', *Revista de Gestão Costeira Integrada*. doi: 10.5894/rgci371.

Chakrabarti, S. K. (2005) ‘Chapter 3 - Ocean Environment’, in *Handbook of Offshore Engineering*, pp. 79–131. Available at: https://www.sciencedirect.com/book/9780080443812/handbook-of-offshore-engineering#book-info.

Challinor, S. and Hall, H. (2008) *Multi-functional artificial reefs scoping study*. London. Available at: http://www.valueofwaves.org/uploads/1/1/4/2/11420190/challinor_2008_artificial_reefs.pdf.

Correia, M. *et al.* (2015) ‘Seahorse (Hippocampinae) population fluctuations in the Ria Formosa Lagoon, south Portugal’, *Fish Biology*, 87(3), pp. 679–690. Available at: https://onlinelibrary.wiley.com/doi/full/10.1111/jfb.12748.

Designboom (2021) *yfalos: modular artificial reef enhances degraded marine ecosystems*. Available at: https://www.designboom.com/design/yfalos-modular-artificial-reef-degraded-marine-ecosytems-topotheque-09-23-2021/.

Düzbastilar, F. O. *et al.* (2006) ‘Recent developments on artificial reef applications in Turkey: Hydraulic experiments’, in *Bulletin of Marine Science*.

Düzbastilar, F. O. and Şentürk, U. (2009) ‘Determining the weights of two types of artificial reefs required to resist wave action in different water depths and bottom slopes’, *Ocean Engineering*. doi: 10.1016/j.oceaneng.2009.06.008.

Dwito Armono, H. and Wirayuhanto, H. (2018) ‘Experimental study of scouring characteristic around hexagonal artificial reef’, in *MATEC Web of Conferences*. doi: 10.1051/matecconf/201817701009.

Evans, A. J. *et al.* (2017) ‘Stakeholder priorities for multi-functional coastal defence developments and steps to effective implementation’, *Marine Policy*. doi: 10.1016/j.marpol.2016.10.006.

Fabio, C. *et al.* (2019) ‘Structural design of an innovative multifunctional artificial reef’, in *OCEANS 2018 MTS/IEEE Charleston, OCEAN 2018*. doi: 10.1109/OCEANS.2018.8604587.

Ferreira, Ó., Dias, J. A. and Taborda, R. (2008) ‘Implications of sea-level rise for continental portugal’, in *Journal of Coastal Research*. doi: 10.2112/07A-0006.1.

Galdo, M. I. L. *et al.* (2022) ‘Definition of an Artificial Reef Unit through Hydrodynamic and Structural (CFD and FEM) Models—Application to the Ares-Betanzos Estuary’. Available at: https://www.mdpi.com/2077-1312/10/2/230.

Garcin, M. *et al.* (2011) *The MOVE coastal erosion case study (Northern Portugal, preliminary results)*, *Univrsidade do Porto*. Available at: https://www.researchgate.net/profile/Manuel_Garcin/publication/263698182_Coastal_Erosion_Vulnerability_Assessment_Northern_Portugal_Case-study_preliminary_results/links/5602718f08ae0b84c4d20bf3/Coastal-Erosion-Vulnerability-Assessment-Northern-Portugal-Ca.

Gattuso, J. P. *et al.* (2018) ‘Ocean solutions to address climate change and its effects on marine ecosystems’, *Frontiers in Marine Science*. doi: 10.3389/fmars.2018.00337.

Gomes, M. C. (2010) *Avaliação dos impactes das condicionantes nas actividades sócio-económicas em áreas marinhas protegidas: caso de estudo na reserva natural da berlenga*. Universidade de Lisboa faculdade de ciências departamento de biologia animal.

Google (2020) *Google earth*.

Granja, H., Monteiro Rodrigues, S. and Danielsen, R. (2016) ‘Changing environments and human settlement during midholocene in rio de moinhos beach (Esposende, northern Portugal)’, *repositório aberto Universidade do Porto*.

Gray, J. S. (1997) ‘Marine biodiversity: Patterns, threats and conservation needs’, *Biodiversity and Conservation*. doi: 10.1023/A:1018335901847.

Harris, L. E. (1995) ‘Engineering design of artificial reefs’, in *Oceans Conference Record (IEEE)*. doi: 10.1109/oceans.1995.528585.

Harris, L. E. (2006) *Artificial Reefs for Ecosystem Restoration and Coastal Erosion Protection with Aquaculture and Recreational Amenities*. Available at: http://www.artificialreef.com/reefball.org/album/%3D%3D) Non-Geographic defined Photos/artificialreefscientificpapers/2006JulyLEHRBpaper.pdf.

Haslett, S. (2008) *Coastal Systems*. London. Available at: https://doi.org/10.4324/9780203893203.

Hixon, M. A. and Beets, J. P. (1989) ‘Shelter characteristics and Caribbean fish assemblages: experiments with artificial reefs’, *Bulletin of Marine Science*.

Hoegh-Guldberg, O. *et al.* (2007) ‘Coral reefs under rapid climate change and ocean acidification.’, *Science (New York, N.Y.)*. doi: 10.1126/science.1152509.

Idealsimulations (2021) *CFD Computational Doamain*. Available at: https://www.idealsimulations.com/resources/cfd-computational-domain/.

Jayanthi, M. *et al.* (2020) ‘Perforated trapezoidal artificial reefs can augment the benefits of restoration of an island and its marine ecosystem’, *Restoration Ecology*, 28(1), pp. 233–243. doi: 10.1111/rec.13041.

Jiamei, W. *et al.* (2020) ‘Study on local scour of artificial reef based on flume test’. doi: 10.12131/20200074.

Jiang, Z. *et al.* (2010) ‘Numerical simulation and experimental study of the hydrodynamics of a modeled reef located within a current’, *Chinese Journal of Oceanology and Limnology*. doi: 10.1007/s00343-010-9228-6.

Jiang, Z. *et al.* (2013) ‘Particle image velocimetry and numerical simulations of

the hydrodynamic characteristics of an artificial reef', *Chinese Journal of Oceanology and Limnology*. doi: 10.1007/s00343-013-2241-9.

Jiang, Z. *et al.* (2016) 'Numerical simulation of effect of guide plate on flow field of artificial reef', *Ocean Engineering*. doi: 10.1016/j.oceaneng.2016.03.005.

Jiang, Z. *et al.* (2020) 'Effect of hole diameter of rotary-shaped artificial reef on flow field', *Ocean Engineering*. Available at: https://www.sciencedirect.com/science/article/abs/pii/S002980181831480X.

Jiang, Z., Liang, Z. and Tang, Y. (2019) 'Numerical analysis of the effect of an inner structure of a cubic frame reef on flow field', *Marine Technology Society Journal*. doi: 10.4031/mtsj.53.2.8.

Joshi, J. B. and Ranade, V. V. (2003) 'Computational fluid dynamics for designing process equipment: Expectations, current status, and path forward', *Industrial and Engineering Chemistry Research*. doi: 10.1021/ie0206608.

Kamath, A. *et al.* (2015) 'CFD investigations of wave interaction with a pair of large tandem cylinders', *Ocean Engineering*. doi: 10.1016/j.oceaneng.2015.08.049.

Kim, D., Jung, S. and Na, W. B. (2021) 'Evaluation of turbulence models for estimating the wake region of artificial reefs using particle image velocimetry and computational fluid dynamics', *Ocean Engineering*. doi: 10.1016/j.oceaneng.2021.108673.

Largier, J. L. (2020) 'Upwelling Bays: How Coastal Upwelling Controls Circulation, Habitat, and Productivity in Bays', *Annual Review of Marine Science*. doi: 10.1146/annurev-marine-010419-011020.

Laurance, W. F. (2010) 'Habitat destruction: Death by a thousand cuts', in *Conservation Biology for All*.

Le, N., Jung, S. and Na, W. B. (2020) 'Wake region estimates of artificial reefs in Vietnam: Effects of tropical seawater temperatures and seasonal water flow variation', *Sustainability (Switzerland)*. doi: 10.3390/su12156191.

Leatherman, S. P., Zhang, K. and Douglas, B. C. (2000) 'Sea level rise shown to drive coastal erosion', *Eos*. doi: 10.1029/00EO00034.

Lee, K. S. and Song, H. K. (2021) 'Automation of 3D average human body shape modeling using Rhino and Grasshopper Algorithm', *Fashion and Textiles*. doi: 10.1186/s40691-021-00249-6.

Leitão, F. (2013) 'Artificial reefs: From ecological processes to fishing enhancement tools', *Brazilian Journal of Oceanography*. doi: 10.1590/S1679-87592013000100009.

Liu, S. *et al.* (2007) 'The hydrodynamic theory, ecological effect and risk

assessment of the artificial fish-reef', in *Proceedings of the International Conference on Offshore Mechanics and Arctic Engineering - OMAE*. doi: 10.1115/OMAE2007-29404.

Liu, Y. *et al.* (2012) 'Numerical simulation and piv study of unsteady flow around hollow cube artificial reef with free water surface', *Engineering Applications of Computational Fluid Mechanics*. doi: 10.1080/19942060.2012.11015440.

Liua, Y. *et al.* (2013) 'A study of the flow field characteristics around star-shaped artificial reefs', *Journal of Fluids and Structures*. doi: 10.1016/j.jfluidstructs.2013.02.018.

Luiyi, H. *et al.* (2017) 'Comparison of Three Ways to Assess the Influence Range of Different Artificial Reefs', *International Journal of Engineering and Technology*. doi: 10.7763/ijet.2017.v9.953.

Maslov, D. *et al.* (2019) 'Experimental testing and CFD modelling for prototype design of innovative Artificial Reef structures', in. doi: 10.1109/oceanse.2019.8867383.

Meesters, E. H. W. G., Smith, S. R. and Becking, L. E. (2015) 'A review of coral reef restoration techniques', *Power System Restoration*.

Munk, W. H. and Traylor, M. A. (1947) 'Refraction of Ocean Waves: A Process Linking Underwater Topography to Beach Erosion', *The Journal of Geology*. doi: 10.1086/625388.

Nixon, S. W. *et al.* (2010) 'Nutrients and the productivity of estuarine and coastal marine ecosystems', *Journal of the Limnological Society of Southern Africa*, 12(1–2), pp. 43–71. doi: 10.1080/03779688.1986.9639398.

Pendleton, L. H. (2004) *Creating Underwater Value: The Economic Value of Artificial Reefs For Recreational Diving*. University of California, Los Angeles.

Puertos del Estado (2022) *Historical data*. Available at: https://www.puertos.es/en-us/oceanografia/Pages/portus.aspx.

Rahman, M. A. A. *et al.* (2021) 'Computational fluid dynamics analysis of rigs-to-reefs (R2R) jacket structures', *CFD Letters*. doi: 10.37934/cfdl.13.1.7283.

Raineault, N. A. *et al.* (2013) 'Interannual changes in seafloor surficial geology at an artificial reef site on the inner continental shelf', *Continental Shelf Research*. doi: 10.1016/j.csr.2013.03.008.

REEF3D (2022) *REEF3D : Open-Source Hydrodynamics*. Available at: https://reef3d.wordpress.com/.

Rijn, L. C. va. (2011) 'Coastal erosion and control', *Ocean & Coastal Management*. doi: https://doi.org/10.1016/j.ocecoaman.2011.05.004.

Van Rijn, L. C. (1993) *Principles of sediment transport in rivers, estuaries and coastal seas*.

Sadrehaghighi, I. (2020) *Mesh Generation in CFD*. Available at: https://www.researchgate.net/publication/318456955_Mesh_Generation_in_CFD.

Santoro, V. c *et al.* (2022) 'Velocity Profiles and Scour Depth Measurements Around Bridge Piers'. Available at: https://onlinepubs.trb.org/Onlinepubs/trr/1991/1319/1319-017.pdf.

Santos, F. D. *et al.* (2014) 'Gestão da Zona Costeira O Desafio da Mudança Relatório do Grupo de Trabalho do Litoral', *Agência Portuguesa do Ambiente, I.P., Comissão de Coordenação e Desenvolvimento Regional do Norte, Comissão de Coordenação e Desenvolvimento Regional do Centro, Comissão de Coordenação e Desenvolvimento Regional de Lisboa e Vale do Tejo, Comissão de Coord*. Available at: https://www.apambiente.pt/_zdata/DESTAQUES/2015/GTL_Relatorio Final_20150416.pdf.

Sayma, A. (2014) *Computational fluid dynamics*. Available at: http://103.47.12.35/bitstream/handle/1/1048/computational-fluid-dynamics.pdf?sequence=1&isAllowed=y.

Schoonees, T. *et al.* (2019) 'Hard Structures for Coastal Protection, Towards Greener Designs', *Estuaries and Coasts*. doi: 10.1007/s12237-019-00551-z.

Shen, R. *et al.* (2020) 'Recent application of Computational Fluid Dynamics (CFD) in process safety and loss prevention: A review', *Journal of Loss Prevention in the Process Industries*. doi: 10.1016/j.jlp.2020.104252.

Sheng, H., Tang, Y. and Wang, X. (2018) 'Relationship between enviromental factors and bentic macroalgea communities of artificial reefs in Laoshan Bay', *Indian jornal of geo marine sciences*.

da Silva, G. V. *et al.* (2020) 'Impacts of a Multi-Purpose Artificial Reef on Hydrodynamics, Waves and Long-Term Beach Morphology', *Journal of Coastal Research*, 95(sp1), p. 706. doi: 10.2112/SI95-137.1.

Silva, P. G. (2019) 'Estudo comparativo do desempenho aerodinâmico de uma turbina eólica de pequeno porte em escala real e modelo reduzido: influência do número de reynolds'. Available at: https://www.lume.ufrgs.br/handle/10183/198554.

Simon Haslett (2016) *Coastal Systems*. university of wales press. Available at: https://books.google.pt/books?hl=pt-PT&lr=&id=MeyVDwAAQBAJ&oi=fnd&pg=PP1&dq=coastal+systems&ots=ufqxFP1OqA&sig=W6cBGhmzSmhgSv-7HWuSyi8qfrg&redir_esc=y#v=onepage&q&f=false.

Tang, Y. *et al.* (2021) ‘Experimental Investigation of Local Scour Around Artificial Reefs in Steady Currents’, *Journal of Ocean University of China*. doi: 10.1007/s11802-022-4883-8.

Vousdoukas, M. I., Almeida, L. P. M. and Ferreira, Ó. (2012) ‘Beach erosion and recovery during consecutive storms at a steep-sloping, meso-tidal beach’, *Earth Surface Processes and Landforms*. doi: 10.1002/esp.2264.

Wang, G. *et al.* (2018) ‘Study on the influence of cut-opening ratio, cut-opening shape, and cut-opening number on the flow field of a cubic artificial reef’, *Ocean Engineering*. doi: 10.1016/j.oceaneng.2018.05.007.

Wang, W. (2020) *Large-Scale Phase-Resolved Wave Modelling for the Norwegian Coast*. Norwegian University of Science and Technology Faculty of Engineering Department of Civil and Environmental Engineering.

Wang, X. *et al.* (2021) ‘Numerical analysis of the flow effect of the menger-type artificial reefs with different void space complexity indices’, *Symmetry*. doi: 10.3390/sym13061040.

Wilson, S. K. *et al.* (2010) ‘Habitat degradation and fishing effects on the size structure of coral reef fish communities’, *Ecological Applications*. doi: 10.1890/08-2205.1.

Yun, D. and Kim, Y. (2019) ‘Scour Characteristics of Artificial Reef through Experiment and Numerical Analysis’, *J. Korean Geosynthetics Society*. Available at: https://doi.org/10.12814/jkgss.2019.18.3.023.

Zhang, J. *et al.* (2021) ‘Numerical Study of Efficiency Indices to Evaluate the Effect of Layout Mode of Artificial Reef Unit on Flow Field’, *Journal of Marine Science and Engineering*. doi: 10.3390/jmse9070770.

9.Appendix

Representation of the results acquired with REEF3D® where a) represent the artificial reefs interaction with a water velocity of 1.9 m/s, b) represent the artificial reefs interaction with a water velocity of 0.88 m/s, c) represent the artificial reefs interaction with a water velocity of 0.7 m/s, d) represent the artificial reefs interaction with a water velocity of 0.33 m/s.

Appendix a)

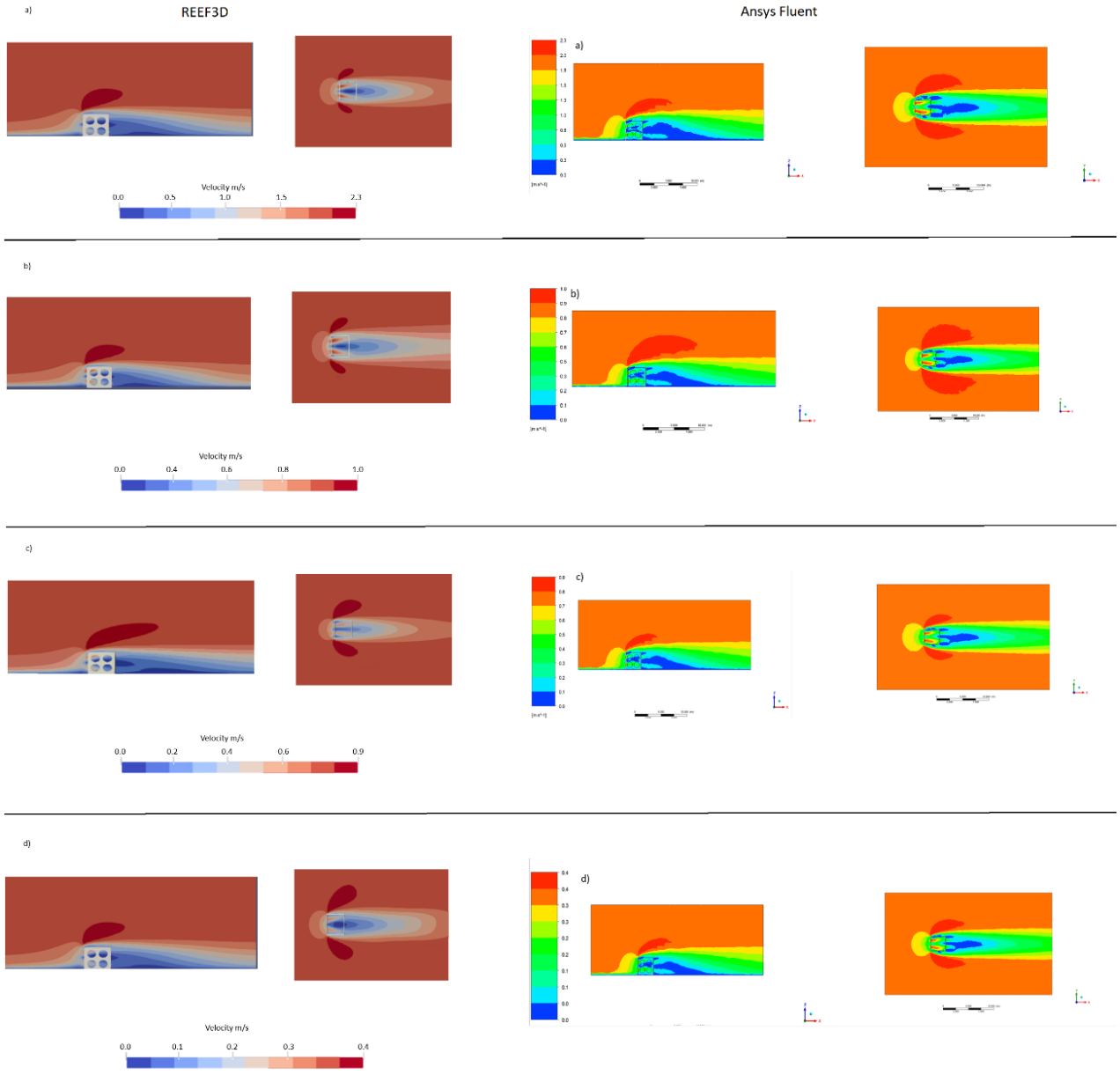
a)
REEF3D
Ansys Fluent
Velocity m/s
0.0 0.5 1.0 1.5 2.3
a)
b)
Velocity m/s
0.0 0.4 0.6 0.8 1.0
b)
c)
Velocity m/s
0.0 0.2 0.4 0.6 0.9
c)
d)
Velocity m/s
0.0 0.1 0.2 0.3 0.4
d)

Appendix b)

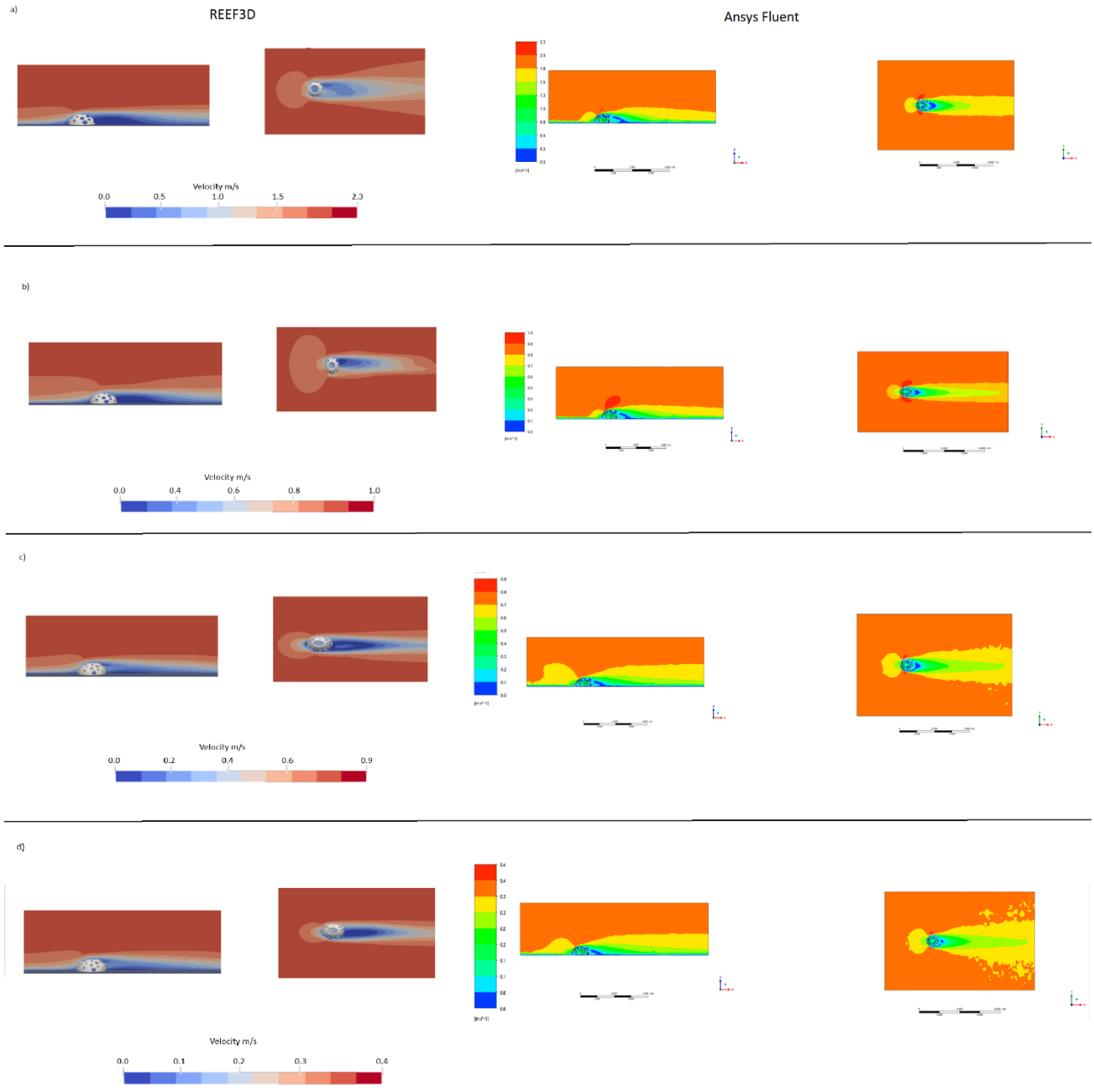
a)
REEF3D
Ansys Fluent
Velocity m/s
0.0 0.5 1.0 1.5 2.3
b)
Velocity m/s
0.0 0.4 0.6 0.8 1.0
c)
Velocity m/s
0.0 0.2 0.4 0.6 0.9
d)
Velocity m/s
0.0 0.1 0.2 0.3 0.4

Appendix c)

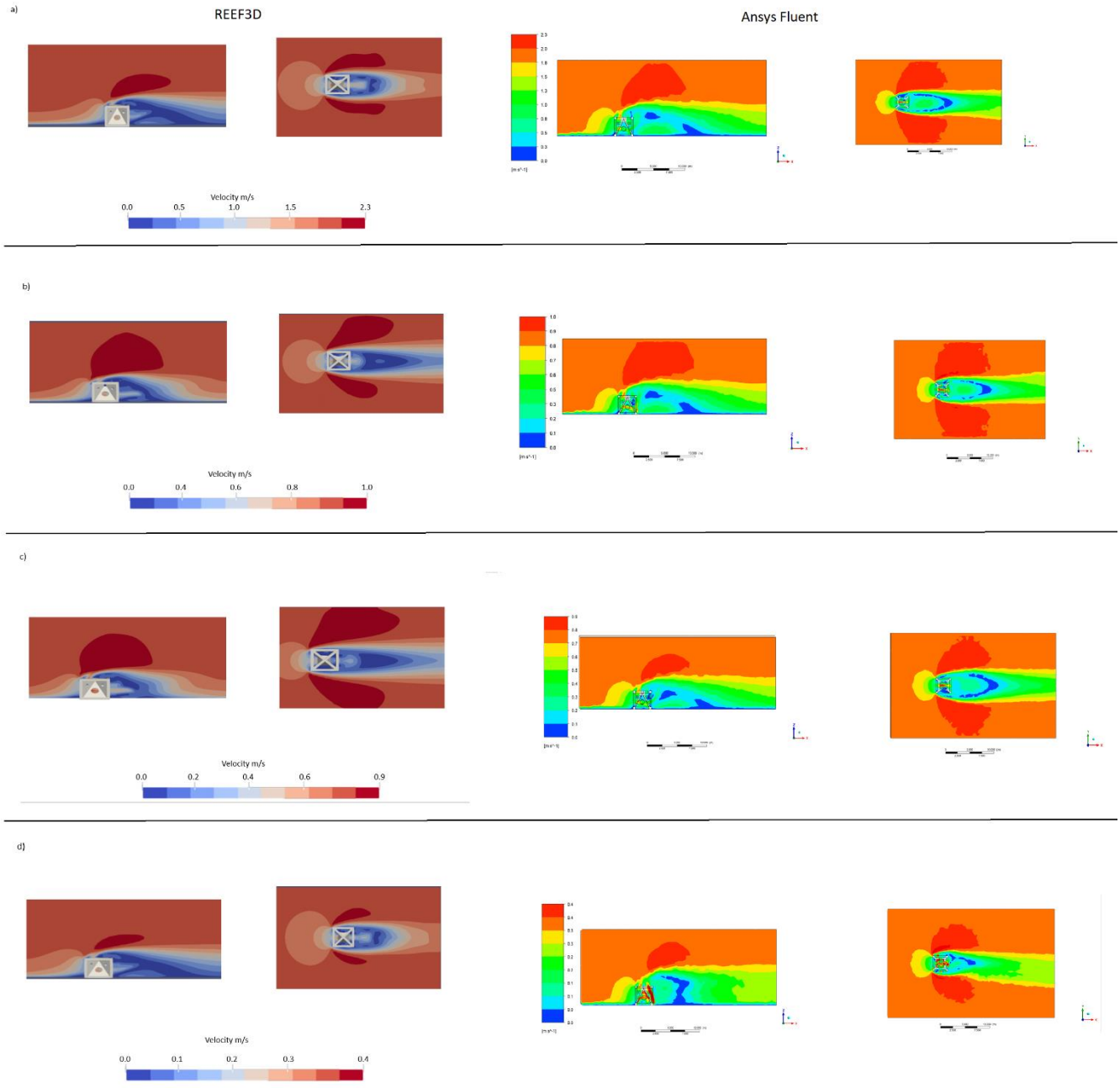
a)
REEF3D
Ansys Fluent
Velocity m/s
0.0 0.5 1.0 1.5 2.3
b)
Velocity m/s
0.0 0.4 0.6 0.8 1.0
c)
Velocity m/s
0.0 0.2 0.4 0.6 0.9
d)
Velocity m/s
0.0 0.1 0.2 0.3 0.4

Appendix d)

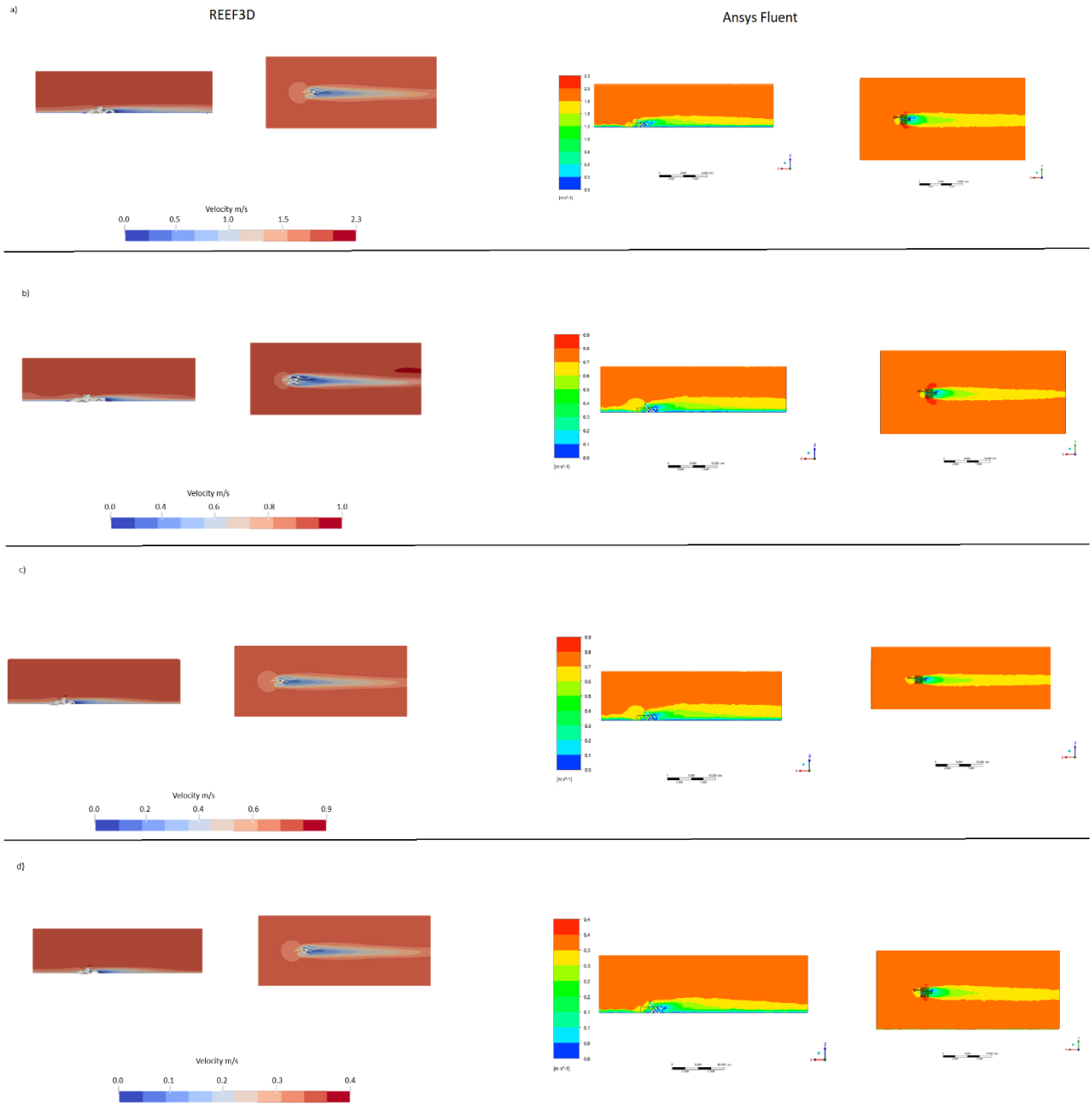
a)
REEF3D
Ansys Fluent
Velocity m/s
0.0 0.5 1.0 1.5 2.3
b)
Velocity m/s
0.0 0.4 0.6 0.8 1.0
c)
Velocity m/s
0.0 0.2 0.4 0.6 0.9
d)
Velocity m/s
0.0 0.1 0.2 0.3 0.4